CHALMERS
UNIVERSITY OF TECHNOLOGY

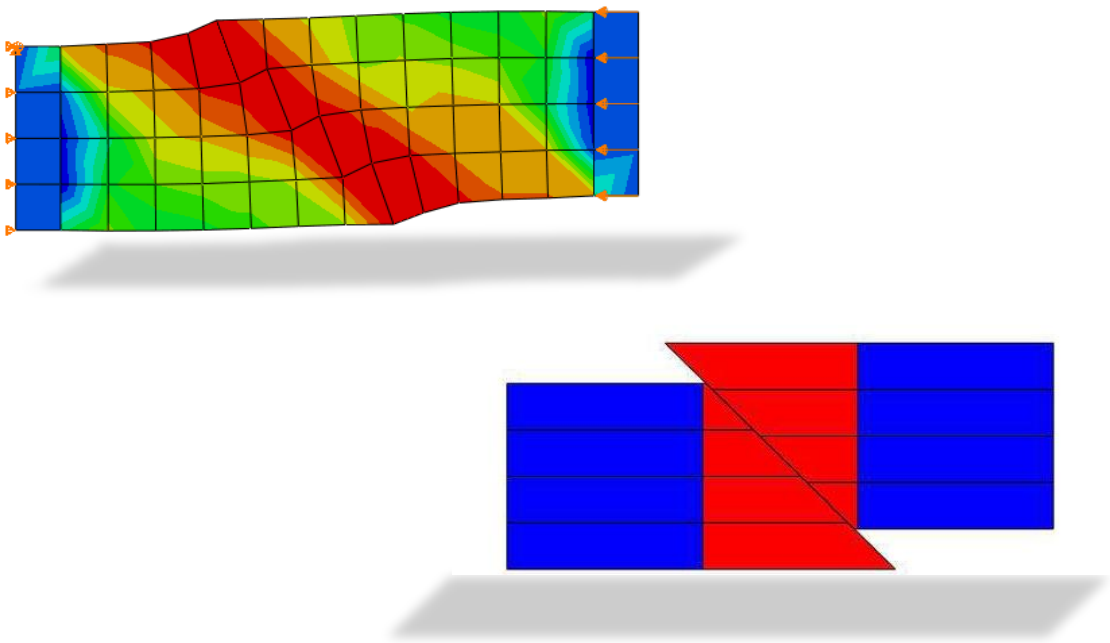

A comparative study on the modeling of matrix cracking in fiber-reinforced polymer laminates under transverse compression

XFEM versus a smeared crack approach

Master's thesis in Applied Mechanics

Ershad Pourbahaaddini, Philip Simonsson

Department of Applied Mechanics
CHALMERS UNIVERSITY OF TECHNOLOGY
Gothenburg, Sweden 2016

MASTER'S THESIS IN APPLIED MECHANICS

A comparative study on the modeling of matrix cracking in fiber-reinforced polymer laminates under transverse compression

XFEM versus a smeared crack approach

Ershad Pourbahaaddini, Philip Simonsson

Department of Applied Mechanics
Division of Material and Computational Mechanics

CHALMERS UNIVERSITY OF TECHNOLOGY
Göteborg, Sweden 2016

A comparative study on the modeling of matrix cracking in fiber-reinforced polymer laminates under transverse compression
XFEM versus a smeared crack approach
Ershad Pourbahaaddini, Philip Simonsson

Master's Thesis 2016:78
ISSN 1652-8557
Department of Applied Mechanics
Division of Material and Computational Mechanics

Chalmers University of Technology
SE-412 96 Göteborg
Sweden
Telephone: + 46 (0)31-772 1000

Cover:
Deformed mesh representation from Abaqus/Explicit simulation using the smeared crack model, and MATLAB simulation using the XFEM approach.

Chalmers repro service / Department of Applied Mechanics
Göteborg, Sweden 2016-09-20

A comparative study on the modeling of matrix cracking in fiber-reinforced polymer laminates under transverse compression
XFEM versus a smeared crack approach
Master's thesis in Naval Architecture and Ocean Engineering
Ershad Pourbahaaddini, Philip Simonsson
Department of Applied Mechanics
Division of Material and Computational Mechanics

Chalmers University of Technology

Abstract

As the number of applications for fiber-reinforced polymers (FRP) is growing, the importance of understanding the failure behavior of this material is rising. This is merely conceivable by developing precise computational material models, which saves time, material, and energy. In general, the polymer matrix is the constitute with the lowest strength against failure in a FRP; hence the matrix requires additional attention especially under transverse compression where it is considered as the principal load carrying component of the FRP. In the present work, a comparative study on the modeling of matrix cracking in FRP laminates under transverse compression is carried out. To do so, an eXtended Finite Element Method (XFEM) approach is developed for discrete crack modeling, and the conventionally used smeared crack approach is applied via an existing Abaqus/Explicit implementation for continuum crack modeling. The comparison of the results illustrates that despite different kinematics behind the models, they both successfully predict a near identical material degradation and energy dissipation in the material response, but with differing predictions when considering frictional tractions and the predicted maximum stress levels. XFEM is established to be mesh-objective and the smeared crack method predicts the material response optimally when the mesh discretization is one element per ply with reduced integration excluding non-linear geometry effects. Moreover, the wedge effect described by geometrical deformation is distinctly represented as cracks are studied explicitly in XFEM, which provides the possibility of further study for inter-laminar effects such as delamination, crack propagation and crack migration.

Key words: XFEM, smeared crack model, progressive damage analysis, transverse compression, friction, fiber-reinforced polymer

Contents

Preface

The current work has been carried out in the Applied Mechanics department of Chalmers University of Technology. Hereby, we would like to acknowledge:

Sincere appreciation to our supervisor and examiner Martin Fagerström and co-supervisor Renaud Gutkin, two respectable and knowledgeable experts in the area of composite materials, for providing the required knowledge and guiding us through accomplishing our master's thesis.

High gratitude towards Swedish Institute (SI.) for awarding the international student of this project with a generous scholarship for his entire two-year master program.

Last but not least, special thanks to our lovely family members for their endless support and motivation not only for this thesis, but also in all aspects of our lives.

Göteborg March 2016-09-20

Ershad Pourbahaaddini, Philip Simonsson

Abbreviation

FRP	Fiber-reinforced polymer
FE	Finite Element
FEM	Finite Element Method
XFEM	eXtended Finite Element Method
GFEM	Generalized Finite Element Method
PUM	Partition of Unity Method
FCM	Fixed Crack Model
RCM	Rotating Crack Model
AE	Artificial Energy
SE	Strain Energy
LEFM	Linear Elastic Fracture Mechanics

1 Introduction

1.1 Background

Energy consumption and environmental effects are becoming more important among all industries. One way of saving energy and lowering emissions is to reduce the structural weight in transportation, and this is applicable by utilizing lightweight high-performance materials while still providing enough strength for the structure. Fiber-reinforced polymers (FRP) are one of the materials to fulfill this purpose best due to their high strength to weight ratio and directional material properties, which can be optimized depending on the loading conditions. These materials are generally characterized by merging separate constituent materials with significantly different physical properties that together produce a material with superior properties.

The major application of composites is focused on military and commercial aircrafts where weight reduction and lowering maintenance cost become even more important. Furthermore, benefits such as weight and assembling cost reduction due to need of fewer joints and connecting components, higher fatigue and corrosion resistance in comparison with metals, especially aluminum, has turned composite materials into a reliable substitute. [1] In automotive industry, the first application of composites was in race-cars. Gradually, the application of composites has been developed and expanded to other vehicles due to their low weight and high performance, which has enabled designers to lower the fuel consumption and design more creative exterior and interior segments. Recently, composites have also been introduced as crash protecting components in cars, and this emphasizes the importance of composite structural integrity and the understanding of laminate failures. In the marine industry reducing carbon footprint and lowering the center of gravity of the vessels by reducing structural weight above the water line are of the main concerns for naval architects. For smaller vessels such as sport and fishing boats and military applications, composites are also used as hull material to fulfill the requirements of the designers. Hence, the request for composite materials is continuously increasing. However, the understanding of composite materials' behavior and response under different loading and environmental conditions, still needs to be developed and improved. Today, the main interests of modern composite material research are related to the modeling of fatigue, creep, energy absorption in collision or impact, and strength reduction due to cracks in structures [1, 2, 3].

For a loaded composite structure, different failure modes may occur depending on the loading conditions due to inhomogeneous characteristics of composites. Generally, these failures are categorized into: fiber breakage, matrix/fiber debonding, delamination, and matrix cracking [4].

One challenging task is to model matrix cracks and consider their effects in FRP laminates under transverse compression that in some cases leads to delamination of plies and thereby structural failure. The key aspect is that matrix cracks formed under transverse compression are inclined with respect to the loading direction (and ply orientation), thus forming a wedge that can initiate and drive delamination growth, see Figure 1-1. Currently, the primary used method in industries to capture this phenomenon is the smeared crack model, in which the crack is studied as a part of the

material model. However, since the formation of a transverse crack in this model is considered as smeared over a volume, it is not clear whether or not this approach can accurately describe the mentioned wedge effect. An alternative to the smeared method can be a discrete and mesh independent approach known as the eXtended Finite Element Method (XFEM), where the crack is introduced and considered as a jump in displacement field while the mesh remains intact, i.e. mesh does not require to follow the crack path. Also the XFEM approach is able to represent the geometrical wedge effect more in details as compared to the smeared crack model. Each of these methods has pros and cons, which will be discussed further in the following sections.

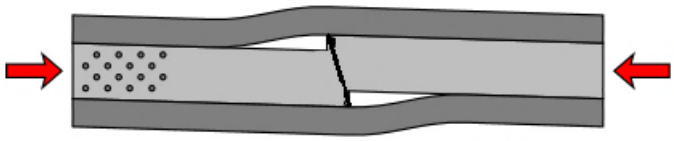

Figure 1-1: Delamination initiated by a matrix crack under transverse compression

1.2 Purpose

The main purpose of this thesis is to investigate any benefits of a more detailed description of ply cracks using the mesh independent method XFEM, in comparison to the modern ply failure modeling that uses the smeared-crack model. Specifically, the purpose is to compare the prediction ability of both methods for a case with compressive loading transverse to the fibers.

1.3 Method

In the current project, initiation and evolution of matrix cracks in a unidirectional fiber-reinforced polymer ply under transverse compression is studied by utilizing the smeared crack model and the XFEM. The implemented model is able to consider damage as well as friction at the material scale. The material properties are provided by Swerea/SICOMP. A similar problem is modeled in two different approaches. One approach is to apply the smeared crack model in Abaqus/Explicit through a subroutine developed by Swerea/SICOMP and written in FORTRAN to investigate the material response and stiffness softening. The other is to utilize a discrete model via a XFEM solver constructed and implemented within MATLAB. To investigate mesh objectivity for both approaches in crack refinements, and to examine geometrical deformations for the wedge effect a mesh study is conducted.

The overview of the stepwise implementation of MATLAB in this thesis can be summarized as:

- A 2D UD FRP ply under prescribed displacements (equivalent to transverse tension) to check stress-strain consistency
- Add discontinuity as a vertical crack using a level-set function and shifted sign enrichment function to check material strain on both sides of the crack interface

- Add linear cohesive behavior at the crack traction in both normal and shearing directions to the crack to check force equilibrium in the domain and specifically find the forces at the crack traction
- Generalize the crack orientation through the domain and consider non-linear crack traction.
- Add non-linear cohesive law which also takes friction into account for the crack traction under negative prescribed displacement (equivalent to transverse compression)

In the end, to evaluate the numerical accuracy and the mesh sensitivity, the final results of the two approaches are compared against each other.

1.4 Limitations

To achieve comparative results for the modeling cases in the given time-frame, a number of simplifications and limitations are applied to the thesis. The assumption and limitations are chosen in a manner such that they do not compromise the validity of the results to any greater extent, and are discussed continuously in the report. The main limitations and assumptions are as follows:

- The studied failure type only includes matrix dominated cracks under transverse compressive loading to the fibers for a single ply.
- The model neglects the lateral stiffness contribution from the adjacent plies, acting as supports on the loaded ply, as well as any other interlaminar effects.
- Internal friction for the crack initiation criterion in the material is not considered, which causes the predicted fracture plane to deviate from a fracture plane in the range of 53 ± 2°, as studied and captured in [5], to the shear dominated failure of 45°.
- The material is assumed to be homogenized and the explicit effects of the fibers are not considered.
- All of the modeling and results will be evaluated through 2D implementations i.e. plane strain condition at the ply cross-section.

2 Theory

To study matrix cracking in a FRP laminate, the material is required to be modeled to capture the mechanical behavior of the material, and this can be done in different approaches. In this chapter energy dissipation and general damage related concepts in material modeling are introduced, as well as two distinctly different approaches are presented; the XFEM and smeared crack approach. Specifically, the focus is on the structure of the XFEM, as well as the description of the smeared crack model, presenting theoretical assumptions and numerical implementations.

2.1 Introduction to material models

The modeling of a structure or specimen is usually done by subdividing it into a finite number of elements consisting of element nodes, and using a constitutive law that defines the relations between the deformations and transmitted forces for the element nodes. Depending on the physical characteristics of the structure, material mechanical behavior can be described by different material models classified in three general categories: continuum models, discrete models, and continuum models with discontinuities. In a continuum model, the material mechanical behavior for an infinitesimal volume of the structure is stated based on the stress-strain relation. However, in a discrete model this behavior, for a set of elements, is described based on the relations between forces and relative displacements or rotations of the elements. A continuum model with discontinuities combines the two previously mentioned models i.e. it utilizes a continuum model for continuous part of the material and a discrete model for the discontinuities within the domain. [6]

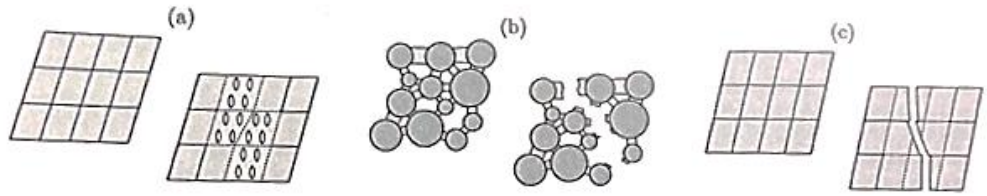

Figure 2-1: Different material models: a) continuum models, b) discrete models, c) continuum models with discontinuities [6]

2.2 Progressive damage modeling

Progressive damage modeling is an effective approach in order to account for the effects of damage and material imperfections on the material stiffness. To set up a progressive damage model for a material, the damage initiation criterion, the energy dissipation mechanics, the damage evolution in the material, and the constitutive models must be properly determined [7].

2.2.1 Damage initiation

Upon damage initiation, the load carrying capacity of the material is decreased as the effect of damage is introduced to the domain. In order to determine when and where a damage is initiated in a loaded material, a damage initiation criterion is required. Typically, the damage is initiated once the stresses in the material reach critical stress levels dependent on the normal and/or shear strengths of the material. For anisotropic materials such as fiber-reinforced polymers, depending on fibers and loading directions and the failure mode, different criteria are used. [8]

2.2.2 Energy dissipation and damage evolution

During the damage process, it can be assumed that the energy is dissipated partly due to the damage evolution and partly due to frictional effects inside the material. The frictional contribution however, becomes more significant in the structures under compressive loads. Damage evolution is generally based on the dissipated fracture energy denoted by G_c during the damage process in the corresponding failure mode. In general, there are three failure modes, mode I to III, also known as opening mode, sliding mode, and tearing mode respectively, see Figure 2-2. The dissipated energy is equal to the area beneath the stress-strain curve corresponding to the failure mode during the damage process, see Figure 2-4. [6, 9]

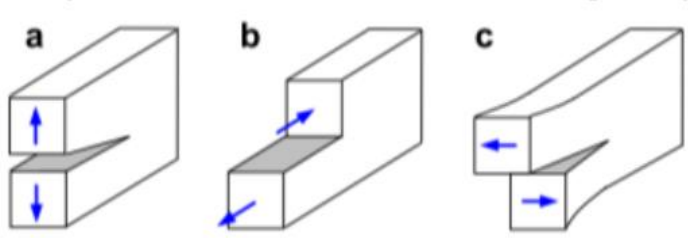

Figure 2-2: Failure modes a) opening mode, b) sliding mode, c) tearing mode [10]

2.2.3 Constitutive damage model

A constitutive law such as Hooke's law for a linear elastic material is valid until the material is intact and no damage is initiated. Thus, stress-strain relation for a uniaxial model as is shown in Figure 2-3 (a) is described as:

$$\sigma = E\varepsilon_e \tag{1}$$

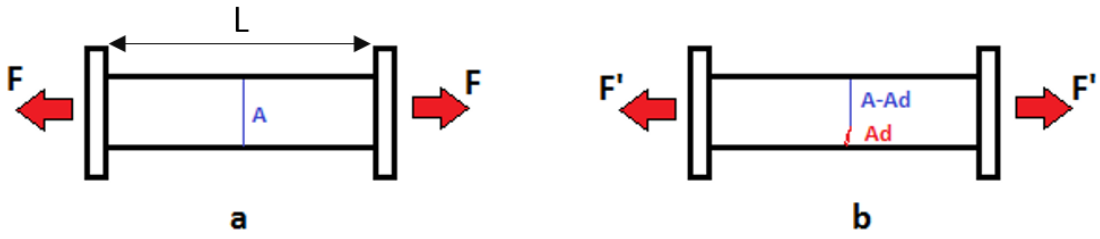

Figure 2-3: Uniaxial loaded bar in a) intact condition, b) damaged condition

If the applied load F increases such that e.g. the principal stress in the material reaches the tensile strength of the material, damage initiates and the load carrying capacity of the material decreases due to the reduction in the intact area in the material from A to $(A - A_d)$, see Figure 2-3. Therefore, a new constitutive law is needed to consider the irreversible effects of the generated micro-cracks on the material stiffness. To account for this degradation, a scalar damage variable is introduced, varying from 0 to 1 for intact and completely damaged material respectively. This scalar variable is then multiplied by the stiffness of the material. The damage variable growth is controlled by the defined displacement for the corresponding failure mode that in the case of uniaxial tension is the opening failure mode. In the simplest case, the degradation can be assumed to behave linearly based on the bi-linear cohesive law, see Figure 2-4. Therefore, Equation (1) can be written as:

$$\sigma = (1 - d)E\varepsilon \tag{2}$$

where d is the scalar damage variable. The corresponding stress-strain relation to the bi-linear cohesive law is illustrated in Figure 2-4. [6]

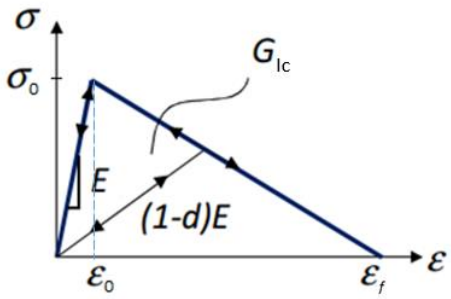

Figure 2-4: Stress-strain relation for bi-linear cohesive law

In general, matrix damage modeling in composite materials, can be done by considering the isotropic effect of the damage caused by an evolving inclined fracture plane with n, t-axes, where the n-axis is normal to the fracture plane and the t-axis is tangential to it, as shown in Figure 2-5. Therefore, the tractions on the fracture plane is written as:

$$\boldsymbol{t} = \begin{pmatrix} \sigma_{nn} \\ \sigma_{nt} \end{pmatrix} = \begin{bmatrix} (1-d)E & 0 \\ 0 & (1-d)G \end{bmatrix} \begin{pmatrix} \varepsilon_{nn} \\ \varepsilon_{nt} \end{pmatrix} \tag{3}$$

where σ_{nn} and σ_{nt} are the normal and the shear traction components and ε_{nt} and ε_{nt} are the normal and the shear strains respectively.

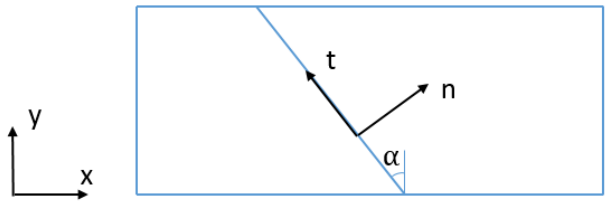

Figure 2-5: Global coordinate system and local coordinate system aligned with fracture plane

Knowing that the material stiffness parallel to the fracture plane remains intact during the damage process and by neglecting the Poisson's effects at the fracture plane the stress-strain relation in Voigt notation can be written as:

$$\underbrace{\begin{pmatrix} \sigma_{nn} \\ \sigma_{tt} \\ \sigma_{nt} \end{pmatrix}}_{\boldsymbol{\sigma^{nt}}} = \underbrace{\begin{bmatrix} (1-d)E & 0 & 0 \\ 0 & E & 0 \\ 0 & 0 & (1-d)G \end{bmatrix}}_{\mathbf{D^d}} \underbrace{\begin{pmatrix} \varepsilon_{nn} \\ \varepsilon_{tt} \\ \varepsilon_{nt} \end{pmatrix}}_{\boldsymbol{\varepsilon^{nt}}} \tag{4}$$

where $\boldsymbol{\sigma^{nt}}$ and $\boldsymbol{\varepsilon^{nt}}$ are the Voigt stress and strain vectors as defined according to the local coordinate system aligned with the fracture plane, $\mathbf{D^d}$ is the constitutive matrix for the damaged material, and d is the scalar isotropic damage variable. Note that for the integration points at the fracture plane, σ_{tt} and ε_{tt} are zeroes.

Finally, stress-strain relation in the global coordinate system xy is obtained by utilizing the transformation matrices for tensors, proposed in literature as:

$$\begin{aligned} \boldsymbol{\sigma^{xy}} &= \mathbf{T_1}^{-1}(\alpha)\boldsymbol{\sigma^{nt}} \\ \boldsymbol{\varepsilon^{xy}} &= \mathbf{T_2}^{-1}(\alpha)\boldsymbol{\varepsilon^{nt}} \end{aligned} \tag{5}$$

$$\mathbf{T_1}(\alpha) = \begin{bmatrix} \cos^2(\alpha) & \sin^2(\alpha) & 2\sin(\alpha)\cos(\alpha) \\ \sin^2(\alpha) & \cos^2(\alpha) & -2\sin(\alpha)\cos(\alpha) \\ -\sin(\alpha)\cos(\alpha) & \sin(\alpha)\cos(\alpha) & \cos^2(\alpha) - \sin^2(\alpha) \end{bmatrix} \quad (6)$$

$$\mathbf{T_2}(\alpha) = \begin{bmatrix} \cos^2(\alpha) & \sin^2(\alpha) & \sin(\alpha)\cos(\alpha) \\ \sin^2(\alpha) & \cos^2(\alpha) & -\sin(\alpha)\cos(\alpha) \\ -2\sin(\alpha)\cos(\alpha) & 2\sin(\alpha)\cos(\alpha) & \cos^2(\alpha) - \sin^2(\alpha) \end{bmatrix} \quad (7)$$

where $\mathbf{T_1}(\alpha)$ and $\mathbf{T_2}(\alpha)$ are the transformation matrices as a function of the fracture plane angle α [11].

2.2.4 Failure modes in composites

For a loaded composite structure, different failure modes may occur depending on the loading conditions due to inhomogeneous characteristics of composites. Generally, these failures are categorized into: fiber breakage, matrix/fiber debonding, delamination, and matrix cracking [4].

Fiber breakage is assumed as the last mode of failure in composites. After fiber breakage, the load carrying capacity of the composite structure is reduced to almost zero.

Matrix/fiber debonding is usually due to the imperfections in the matrix and fiber bonding, which results in strength reductions of the composite laminate. The manufacturing of composites must be done such that this phenomenon does not occur before matrix cracking and delamination.

Delamination is a phenomenon in which the interface between two or more plies in a composite laminate is demolished and plies become separated. Delamination results in severe stiffness reduction or even brittle fracture. It is normally initiated by stress concentrations that can be caused by defects or circumstantial conditions such as manufacturing errors, moisture, etc.

Matrix cracking is of high degree of importance, particularly when a composite ply is loaded transversally to the fiber orientation. In this condition, the matrix can be regarded as the only load-carrying component and, typically, the matrix has the lowest strength in composite laminates. This is due to the brittle nature of the matrix and can result in other modes of failure e.g. delamination.

2.3 Continuum damage modeling

In continuum models, the constitutive relation is typically constructed based on a stress-strain relation for an infinitesimal volume of a structure. One of the continuum models conventionally used in industry is known as the smeared crack model, which is discussed more in details in the following subsection.

2.3.1 Smeared crack model

The smeared crack model was primarily introduced to study the fracture of concretes under tensile loading. At first, the cracks orientations were assumed to be fixed, later, the rotating crack model was also introduced. [6] Today, this method is applied to other materials such as metals and composites as well. In this model, it is assumed that countless generated micro-cracks are smeared throughout the material while in the discrete models, a crack is considered as a discrete discontinuity line, see Figure 2-6. The smeared crack model therefore accounts for material mechanical behavior by defining the influence of the existing cracks as a stiffness softening in the material, without a discrete description of the crack itself. Thus, this approach can be considered as a continuum material model.

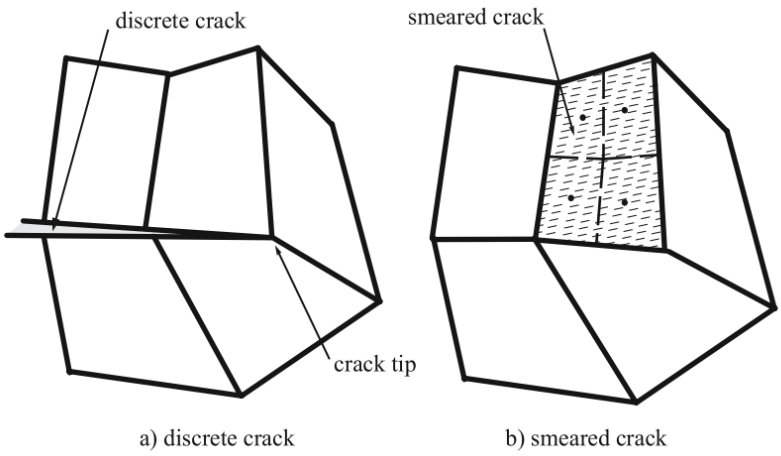

Figure 2-6: Crack models for typical finite element mesh [4]

2.3.1.1 One-dimensional model

In the smeared crack model, the total strain of the component can be decomposed into two parts, one part related to the intact material, which in general, may be governed by nonlinear constitutive relation but usually is assumed to be linear elastic, and the other part related to the crack openings. Therefore, strain decomposition can be written as:

$$\varepsilon_{tot} = \varepsilon_e + \varepsilon_c \tag{8}$$

where ε_e is the elastic strain and ε_c is the crack strain due to cracks opening, see Figure 2-7. The elastic strain can be computed by utilizing Hooke's law as in Equation (1).

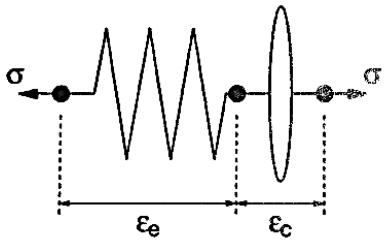

Figure 2-7: Schematic representation of smeared crack model as an elastic unit coupled in series to a crack unit [6]

It is assumed that for an intact material, the crack strain is zero and crack initiation occurs when the driving stress reaches the corresponding strength of the material. Up to this level of stress, linear elastic constitutive relation is applicable. However, upon crack initiation a new constitutive relation is required to capture the material mechanical behavior. To define the new constitutive relation, the micro-cracks are replaced with an equivalent cohesive crack that can transmit stress. This cohesive stress can be assumed to be a function of the crack strain and be written as:

$$\sigma = f_c(\varepsilon_c) \tag{9}$$

where f_c is identified based on experiments.

One drawback of this relation is its dependency on strain gauge length, as the gauge length in experimental measuring data could vary. An alternative to this method is the traction-separation law which assumes cohesive stress as a function of the crack opening, ω. Therefore, it can be considered as gauge length independent and be written as:

$$\sigma = f_\omega(\omega) \tag{10}$$

where f_ω is the softening function. There are several choices of representing a softening law, which is further described in Section 2.4.2.

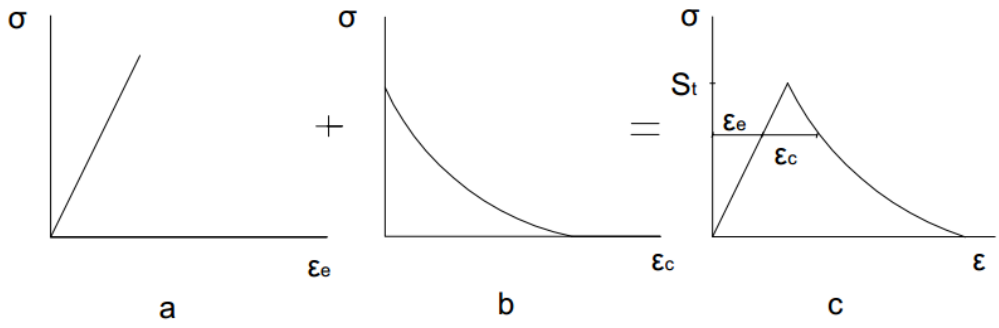

Figure 2-8: a) Linear-elastic relation for intact material, b) stiffness softening upon crack initiation, c) stress vs - total strain curve

2.3.1.2 Three-dimensional model

For three-dimensional models Equation (8) and (1) can be written generally as:

$$\boldsymbol{\varepsilon}_{\mathbf{tot}} = \boldsymbol{\varepsilon}_{\mathbf{e}} + \boldsymbol{\varepsilon}_{\mathbf{c}} \tag{11}$$

$$\boldsymbol{\sigma} = \mathbf{D}_{\mathbf{e}}\boldsymbol{\varepsilon}_{\mathbf{e}} \tag{12}$$

where $\mathbf{D}_{\mathbf{e}}$ denotes the constitutive relation matrix.

For model simplification, the micro-cracks in the material can be substituted with an equivalent planar crack with a normal vector $\mathbf{n} = (1 \quad 0 \quad 0)^T$. Thus, the traction on the crack face can be written as:

$$\mathbf{t}_{\mathbf{c}} = \boldsymbol{\sigma} \cdot \mathbf{n} \tag{13}$$

One can introduce the local coordinate system as shown in Figure 2-9 that aligns with the crack with the unit vector **n** normal to the crack face, and **t** and **l** orthogonal unit vectors in the crack plane.

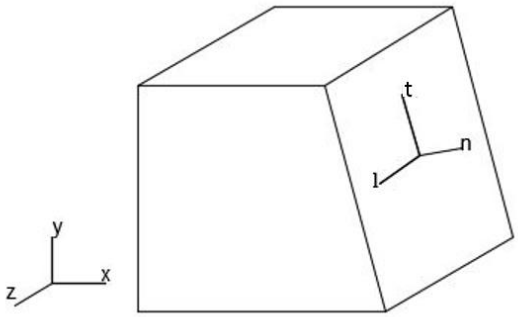

Figure 2-9: Local coordinate system (nlt) on the equivalent planar crack plane

Accordingly, the strain in the crack plane can be expressed in terms of normal strain ε_{nn} contributed by the crack opening and shear strains γ_{nt} and γ_{nl} contributed by sliding in **t** and **l** direction respectively. Therefore, the crack strain vector can be expressed as:

$$\mathbf{e}_{\mathbf{c}} = \varepsilon_{nn}^{c} n + \gamma_{nt}^{c} m + \gamma_{nl}^{c} l \tag{14}$$

Note that the traction components are functions of the crack opening and sliding by the generalized form of cohesive law. Also $\mathbf{e_c}$ is zero for an uncracked material.

Upon crack initiation there are two possibilities for the equivalent planar crack orientation and propagation:

- It can be assumed that all micro-cracks have the same orientation and the crack orientation remains fixed after initiation. As a consequence, for the equivalent planar crack, all traction components are linked with all crack strain components. This model is known as Fixed Crack Model (FCM).

- It is rare that all micro-cracks appear in the same orientation, therefore, Rotating Crack Model (RCM) is introduced to consider the possibility of various crack orientation by adjusting the orientation of the equivalent crack. Adjustment is done by assuming that the crack normal vector is always aligned with the maximum principal strain. Consequently, the shear strain γ_{nt} and γ_{nl} and crack traction components σ_{nt} and σ_{nl} are zero. Hence, cohesive stress law for the stiffness softening is reduced to [6]:

$$\sigma_{nn} = f_c(\varepsilon_{nn}^c) \tag{15}$$

  Although this model is physically more realistic than FCM, computational costs are increased dramatically. Also considering the fact that composites typically have a very small ply thickness, it is concluded that the results from FCM are sufficiently promising in the modeling of cracks through the ply thickness.

2.3.2 Strain localization

Damage initiation in materials subjected to non-homogeneous deformation may cause strain localization. The strain localization is presented in the form of a shear band, in which extreme straining may cause some variable fields to be discontinuous. This phenomenon is resulted from the stiffness softening in the material, as explained in Section 2.2, and normally leads to the fracture of the structure. The gradient of softening and energy dissipation during the damage process is highly dependent on the mesh size in finite element modeling. [8, 12]

2.3.2.1 Inobjectivity of strain-softening continuum

To see the inobjectivity of the strain softening, consider the bar in Figure 2-3 subjected to uniaxial tension is decomposed into N_e elements as is shown in Figure 2-10. It is assumed that the bar behaves linearly elastic up to a peak stress, σ_0, where the damage initiation results in linear softening up until a fracture point corresponding to ε_f, see Figure 2-4.

Figure 2-10: The meshed bar with 3 elements

Considering that material properties and dimensions are not always perfectly uniform, it can be assumed that a part of the material has a strength slightly lower than the strength of the rest of the material due to a local defect. Hence, upon damage initiation at the local weaker part with the peak stress σ_0 and corresponding strain ε_0, two different phenomena occur in the material; the weaker part experiences softening with an increase of strain, whilst the stronger parts starts to elastically unload with a decrease of strain. Considering static force equilibrium, the stress profile must be uniform throughout the bar while strain profile is not uniform and has two valid strain corresponding to a certain stress $\bar{\sigma}$, see Figure 2-11 (a). Let us denote the total length of the softening region by L_s and the total length of unloading region is as $L_u = L - L_s$. Consequently, the total elongation of the bar u_{tot} is computed as:

$$u_{tot} = L_s\varepsilon_s + L_u\varepsilon_u \tag{16}$$

where ε_s is the strain in the softening region and ε_u is the strain in the unloading region. At the fracture point where the stress is totally relaxed, ε_u goes to zero, thus $u_f = L_s\varepsilon_s = L_s\varepsilon_f$. Now the problem arises since the length L_s is not known and it can be any value between zero to L. Hence, the problem has infinite number of solutions depending on the length L_s, see Figure 2-11 (b).

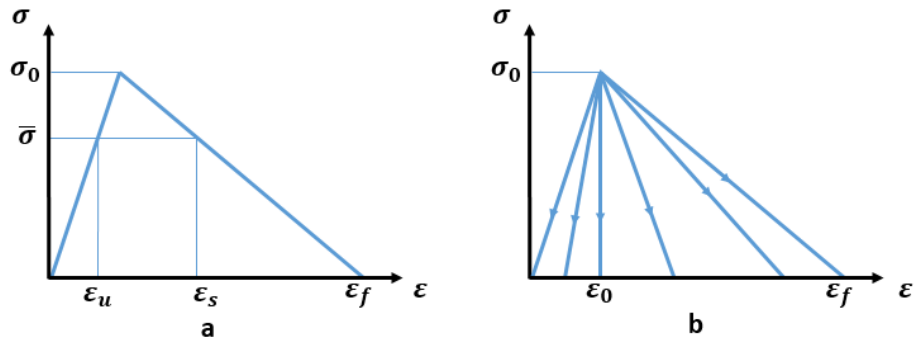

Figure 2-11: a) Stress-strain diagram with linear softening, b) different possible post-peak stress relaxation

Suppose that the weak part of the bar is located in the middle and occupies N_d elements as is indicated in Figure 2-12 by red color. Therefore, the total length of the softened region is as:

$$L_s = \frac{N_d * L}{N_e} \tag{17}$$

N_d is highly dependent on the mesh size, and for a refined mesh, see Figure 2-12 (b), strain is localized in a smaller portion of the elements. Consequently, L_s is reduced and energy dissipation and the required external work during the damage process are also reduced by mesh refinement. [6] To demonstrate this reduction, results for three different mesh sizes are extracted from [8] and shown in Figure 2-13.

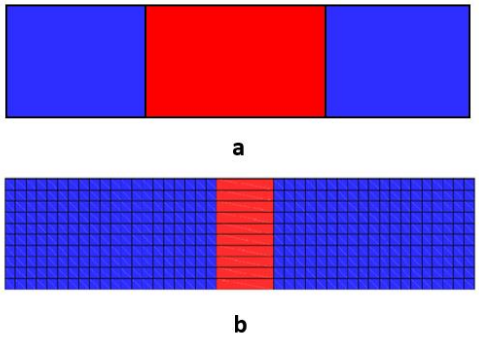

Figure 2-12: Strain localization in N_d damaged elements indicated by red color for a) course mesh, b) fine mesh

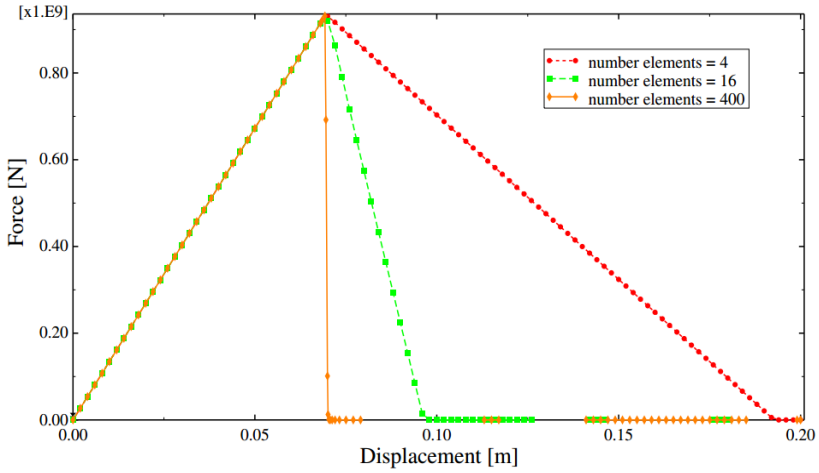

Figure 2-13: Force-displacement diagram for three different mesh sizes

2.3.2.2 Mesh adjustment

To obtain a mesh-independent model and avoid inobjectivity of strain-softening, element size must be taken into consideration. Bazant in [13] introduced the crack band model in which the line cracks in the material are substituted by a band of paralleled micro-cracks in the damaged elements with the width denoted by w_c, see Figure 2-14 (a) and (b). The crack band modeling is computationally more efficient than the line crack modeling. In this model, the fracture strain is dependent on the fracture toughness of the material in the corresponding failure mode e.g. opening failure mode is defined as:

$$\varepsilon_f = 2\frac{\left(\frac{G_{Ic}}{l_c}\right)}{\sigma_0} \tag{18}$$

where l_c is the characteristic length of elements, and σ_0 is the peak stress corresponding to the damage initiation strain ε_0.

For a geometry with uniform square mesh with the case that crack band is straight, l_c is equal to the element size h. However, for the cases that the crack generates a zig-zag crack band as is shown in Figure 2-14 (c), the characteristic length is adjusted as:

$$\begin{aligned} l_c &= \frac{h}{\cos(\alpha)}, \qquad 0 \le \alpha \le 45° \\ l_c &= \frac{h}{\sin(\alpha)}, \qquad 45 \le \alpha \le 90° \end{aligned} \tag{19}$$

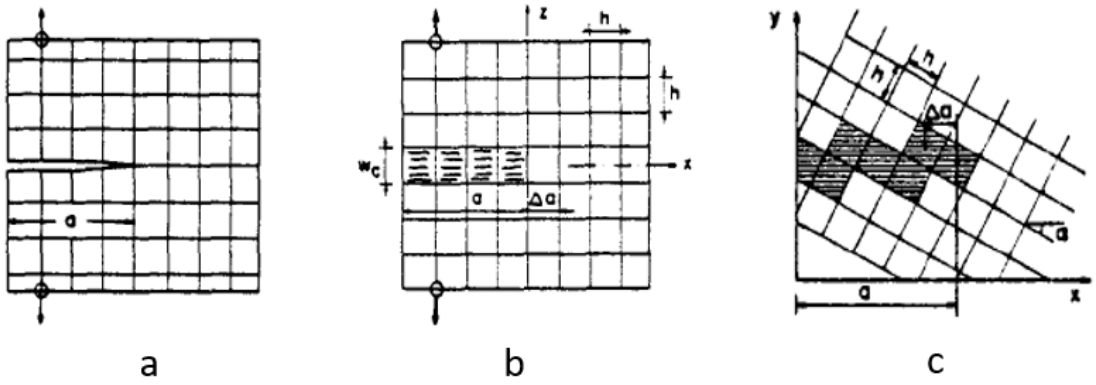

Figure 2-14: a) Line crack model, b) crack band model, c) zig-zag crack band [13]

Utilizing the mesh adjustment, the fracture energy is adjusted to the mesh size and the results for different mesh sizes become identical, see Figure 2-15.

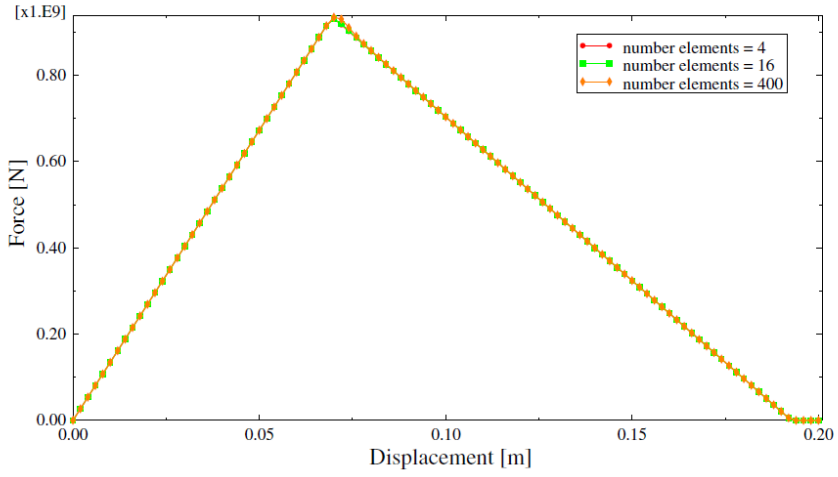

Figure 2-15: Force-displacement diagram with mesh adjustment for three different mesh sizes [8]

2.4 Discrete damage modeling

In discrete models the material behavior is described based on the relations between forces and relative displacements, or rotations, of the elements for a set of elements. The classical standard finite element approximation is based on properties of polynomials, which implies that its accuracy is optimal only for smooth solutions. Therefore, the existence of inner-element kinks, jumps, or singularities at some interface causes a significant decrease in accuracy for this method. In order to capture these kinks or jumps, element edges in the mesh must then coincide with the interface of the discontinuities. Thus, the need for modifying the mesh requires manual adjustment to align with the interface, which may require continuous interface tracking for moving interfaces, in order to refine the mesh near discontinuities. Hence, the application of standard FE approximation is limited. An alternative is to introduce additional terms, also known as enrichment terms, to the classical finite element approximation, which enables non-smooth solutions to be captured within a fixed mesh. This method is referred to generally as enriched FEM and is able to approximate any kind of non-smooth solutions, due to inner-element discontinuities, accurately. [14, 15]

2.4.1 Introduction to discontinuities and high gradients

Generally, in material applications, there are examples that the field quantities or their gradients change intensely over a small length of δl with respect to the considered domain. Depending on the δl, modeling of the phenomena can be subdivided into the following categories: 1) δl is zero or almost zero, for which it should be considered as discontinuity, 2) δl is small and can be considered continuous, although, it leads to local high gradients. High gradients usually occur along interfaces or singularities.

2.4.1.1 Interfaces

Interfaces are the points, lines, or areas depending on the domain dimension, where two or more systems or sub-domains meet, and are always one order less in dimensions than the domain that they are in. For instance, in a 3D domain interfaces are surfaces and in a 2D domains they are lines.

In general, interfaces are categorized into open and closed interfaces. Open interfaces are characterized by discontinuities that either starts or ends within the domain with one or several tips, see Figure 2-16 (a). On the contrary, closed interfaces are characterized by closed end discontinuities without any additional effect of singularities from crack tips, e.g. voids, holes, or crack throughout the domain, see Figure 2-16 (b). [14]

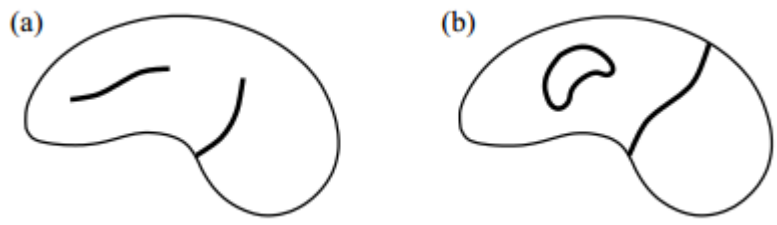

Figure 2-16: a) Open interfaces, b) closed interfaces

Modeling of domains with interfaces usually has non-smooth solutions. Generally, there are two approaches to approximate non-smooth solutions: One is a mesh dependent method based on polynomial approximation spaces and standard FEM shape functions, in which the mesh must be aligned with the interface and refined around singularities to have a smoother solution. The second approach is a mesh independent method in which the polynomial approximation space, with standard FEM shape functions, is enriched with additional enrichment terms in order to capture smooth solutions around discontinuities. [14] The enrichment terms are governed by shape functions that can be the same as classical finite element shape functions or defined differently depending on the type of discontinuity.

2.4.1.2 Discontinuities

Discontinuities are generally categorized into strong and weak discontinuities. The solution for a strong discontinuity contains a jump in the field quantities, e.g. displacements, along with corresponding singular gradients, e.g. strains, alongside the interface, see Figure 2-17 (a). For weak discontinuities, the solution is described as a kink, i.e. the field quantities are still considered continuous whilst their gradients are not, see Figure 2-17 (b). [14] Multi-material models are considered as typical examples of weak discontinuities, whereas through the thickness cracks are examples of strong discontinuities. Both strong and weak discontinuities can be considered as closed or open interfaces.

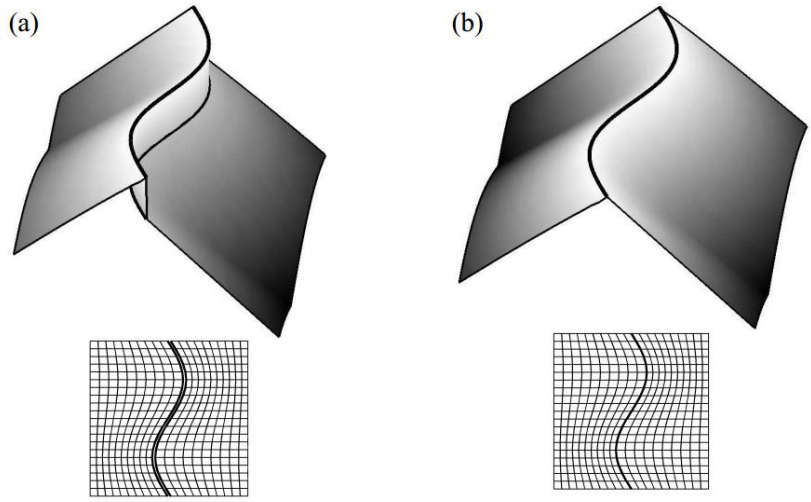

Figure 2-17: Representation of a) Strong discontinuity, b) Weak discontinuity [14]

2.4.1.3 Level-set function

One way of determining the position of the interface in finite element approximation is to introduce a level-set function Γ_{12} in the domain Ω to distinguish the sub domains Ω_1 *and* Ω_2 on the sides of an interface. A level-set function is a continuous function which is negative on one side of the interface, positive on the other side, and zero on the interface, see Figure 2-18.

One type of level-set functions is the signed distance function defined as:

$$\phi(x) = \pm \min_{x^* \in \Gamma_{12}} \|x - x^*\| \ , \qquad \forall x \in \Omega \tag{20}$$

where $\|\cdot\|$ is the Euclidean norm and x is the closest point to x^* on the interface. Figure 2-18 (b) illustrates a graphical representation of the signed distance function. The level-set function is useful especially for discrete crack modeling to find out which elements in the domain must be enriched and how. [14]

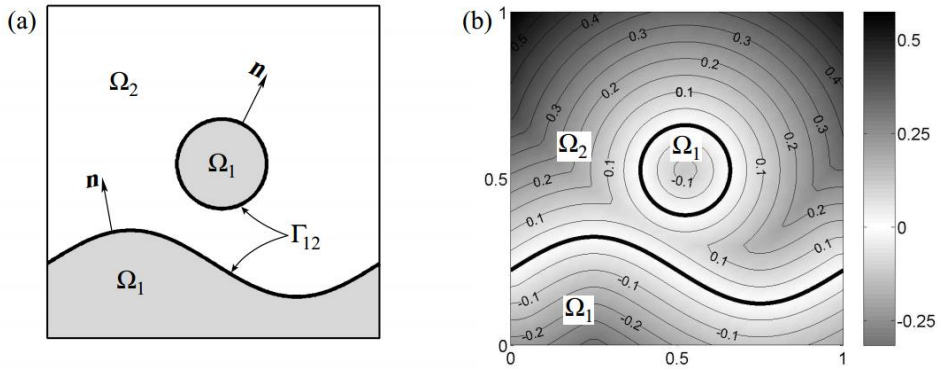

Figure 2-18: a) Domain decomposition by introducing level-set function Γ_{12} , b) the signed distance function [14]

2.4.1.4 Structure of enriched FEM

In general, classical finite elements can be enriched extrinsically in such a way that new shape functions are added to the standard shape functions in the enriched elements. These shape functions are not necessarily the same as the standard shape functions. As a result of the added terms, new unknowns are also added to the approximation. An alternative is to enrich classical finite elements intrinsically such that all or some of the standard shape functions are replaced by new shape functions to capture the smooth solution around discontinuities. Unlike extrinsic enrichment, in intrinsic enrichment the number of shape functions and unknowns are unaltered since the shape functions are just replaced and not added.

Enrichments can also be categorized into global or local enrichment. The enrichment is global when all elements in the observed domain are enriched, or local when just a part of the domain is enriched. Global enrichment is usually applied to models for which the solution is globally non-smooth, e.g. in high-frequency solutions. [14] However, approximations based on global enrichments typically require considerable computational resources due to the drastic increase in the number of degrees of freedom added to the domain. This is because the degrees of freedom are proportional to the number of enriched nodes. In general, discontinuities and high gradients of field quantities are more accurately represented as physical localized phenomenon. The approximation of such phenomenon with a global approximation space is therefore clearly not efficient. Thus, in crack modeling it is computationally beneficial and more justifiable to introduce local enrichments. [14, 16]

Although there are some examples of utilizing XFEM for cases that are enriched globally, XFEM is utilized as local enrichment for the rest of this thesis.

2.4.2 XFEM

A standard extended finite element approximation of a function $u^h(x)$, also known as XFEM, utilizes local enrichment of nodes in a subset of the domain ($I^* \epsilon I$) and have the form:

$$u^h(x) = \sum_{i \epsilon I} N_i(x) u_i + \sum_{i \epsilon I^*} N_i^*(x) \cdot \psi(x) a_i \tag{21}$$

where the first term is the standard FE approximation and the second term is the added enrichment, with the coefficients u_i and a_i representing nodal unknowns of standard FE and enrichment at node i, respectively. The function $\psi(x)$ is the enrichment function and includes specific information about the discontinuity, which is then added into the approximation space. The functions N_i^* are standard shape functions, often chosen to be equivalent to the standard FE shape functions, as in Equation (21), but are necessarily not the same.

These functions N_i^* then build what is known as the concept, partition of unity (PU), over the enriched elements in the subdomain I^*. The basis of any enrichment approximation is realized through the partition of unity concept, where PU is crucial to the structure of the enrichment and the accuracy of the solution. PU is generally expressed in the form:

$$\sum_{i \epsilon I^*} N_i^*(x) = 1 \tag{22}$$

By having a complete partition of unity in the enriched areas, the FE approximation of Equation (21) can reproduce any enrichment function exactly in the domain I, and thus ensuring reliable terms in the approximation space. However, when not able to fulfill the condition of Equation (22), the terms in the approximation space are not completely reliable, and the utilization of XFEM is no longer straightforward. [14, 17]

2.4.2.1 Shifted enrichment functions

In standard FE approximations, as described as the first term in Equation (21), the shape functions have what is known as the Kronecker-δ property, which is described as:

$$N_i(x_j) = \delta_{ij} = \begin{cases} 0 & : i \neq j \\ 1 & : i = j \end{cases} \tag{23}$$

However, approximations of the form Equation (21) together with the enrichment function $\psi(x)$, generally do not have the Kronecker-δ property. Consequently, $u^h \neq$

u_i and the wanted function values of $u(x)$ at a specific node k is no longer directly known as u_k. This complicates the imposition of Dirichlet boundary conditions, and is similar to the situation of mesh-free approximations, where the shape function associated to a node does not vanish at other surrounding nodes. [18] Conversely, by modifying the approximation and finding enrichment functions that are zero at all other nodes, it follows from standard FEM that $u^h(x_k) = u_k$. This is achieved by shifting the enrichment approximation as:

$$\psi^{shift} = [\psi(x) - \psi(x_i)] \tag{24}$$

and following the formulation of standard XFEM in Equation (21), using ψ^{shift} instead of $\psi(x)$, the approximation then becomes:

$$u^h(x) = \sum_{i \epsilon I} N_i(x) u_i + \sum_{i \epsilon I^*} N_i^*(x) \cdot [\psi(x) - \psi(x_i)] a_i \tag{25}$$

and thus recovering the Kronecker-δ property. This therefore enables the following properties to hold in the approximation:

i) $u^h = u_i$, where the computed unknowns are directly the function values of $u(x)$ at node i.
ii) Imposing the Dirichlet boundary conditions $\hat{u}(x)$ is straightforward: $u_i = \hat{u}(x_i)$.

Furthermore, by shifting the enrichment, there are additional numerical benefits for the issue of blending elements, and is further described in Section 02.4.2.3. [19, 20]

2.4.2.2 Strong discontinuity enrichments

In XFEM, the approximation of discontinuities is based on the shape functions with the use of enrichment functions. In the presence of strong discontinuities in the domain such as cracks, typical choices for the enrichment function $\psi(x)$ is the sign of the level-set function, $\phi(x)$:

$$\psi(x) = sign\big(\phi(x)\big) = \begin{cases} -1 : \phi(x) < 0 \\ 0 : \phi(x) = 0 \\ 1 : \phi(x) > 0 \end{cases} \tag{26}$$

or the Heaviside function:

$$\psi(x) = H\big(\phi(x)\big) = \begin{cases} 0 : \phi(x) \leq 0 \\ 1 : \phi(x) > 0 \end{cases} \tag{27}$$

where both can be considered as step enrichment functions. By introducing a discontinuity in a simple one-dimensional domain, as seen in Figure 2-19, the two

enrichment functions simulate the discontinuity differently, as according to Figure 2-20.

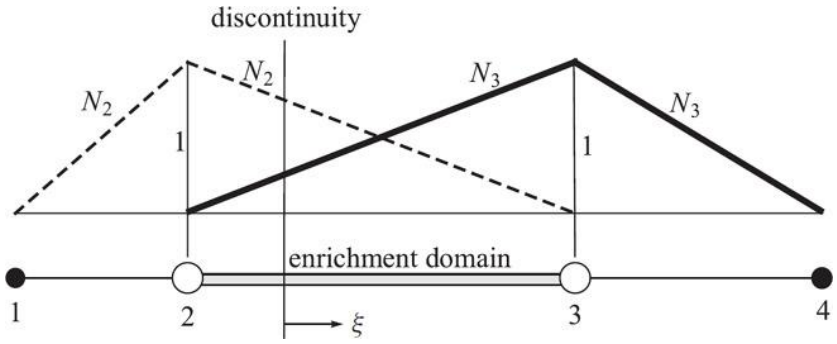

Figure 2-19: A one-dimensional example of ordinary shape functions N and the discontinuity, starting from ξ, on the enriched domain [4]

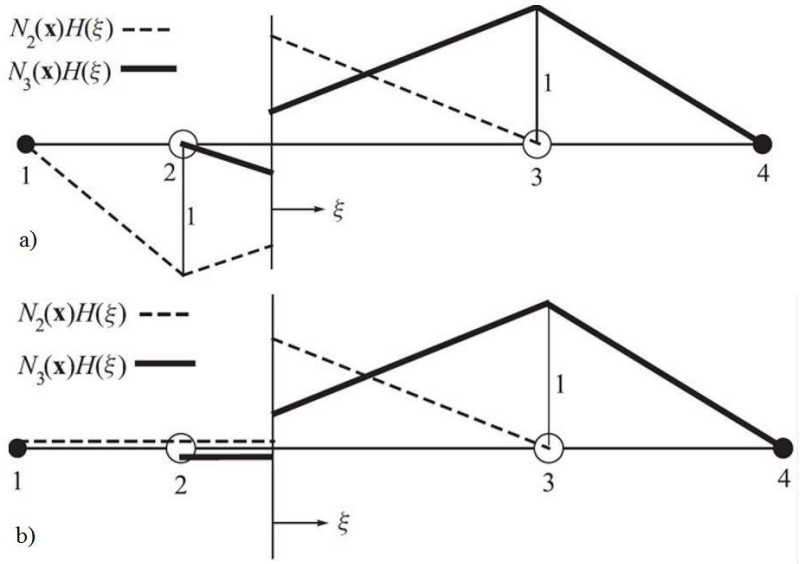

Figure 2-20: The effect of a) sign and b) Heaviside enrichments for the one-dimensional example [4]

It is important to note that both sign and Heaviside step enrichments produces identical results after numerical implementation, as they both span the same approximation space. [4]

2.4.2.3 Blending elements

As a consequence of enriching a specific subset of nodes ($I^* \epsilon I$) with local enrichments, each element in the domain falls into one of the following categories:

i) standard FEM with none of the nodes enriched
ii) a reproducing element with all of the nodes enriched
iii) a blending element with some of the nodes enriched

which can be seen in Figure 2-21, where (a) is a 2D representation of all the element categories with the nodal subset choice of I^*. In (b), reproducing elements are shown

to be able to fulfill the criterion to build a complete partition of unity, visualized as a flat top. However, this is generally not the case for the blending elements.

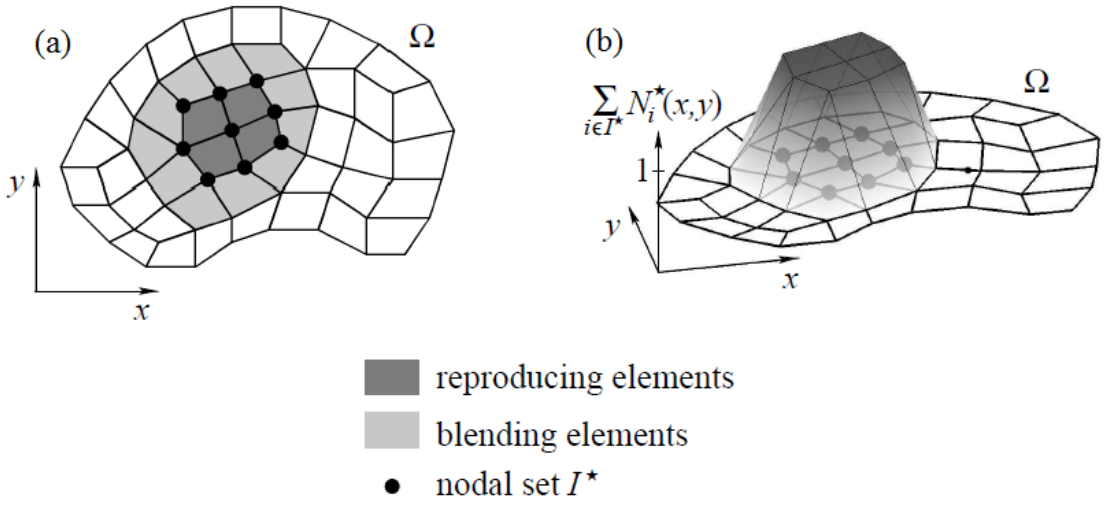

Figure 2-21: Domain in two dimensions with nodal subset I^*, a) enriched nodes and elements due to choice of I^*, b) the functions $N_i^*(x)$ with partition of unity in reproducing elements but not blending elements [14]

It is of importance to acknowledge the situation of blending elements due to local enrichments, where, the functions $N_i^*(x)$ are non-zero and do not build a partition of unity as only a few nodes being enriched. The failure to satisfy the partition of unity has two important implications:

i) The enrichment function cannot be reproduced exactly in the subdomain by the enriched approximation.
ii) Additional unwanted terms are added to the approximation space.

where these unwanted terms are shown to affect all enriched elements and may decrease the convergence rate and reduce accuracy of the XFEM approximations drastically depending on the choice of enrichment. [17] Moreover, the influences of these unwanted terms are generally not easily predicted. Thus, while standard XFEM is proposed to improve accuracy and approximation by local enrichments, the overall improvement can be minor due to the effect of blending elements. However, there are ways of coping with the issue of blending elements to improve the approximation scheme, and for enrichment functions that are zero or constant in the blending elements no effects of any unwanted terms are present. [14, 21]

There are several approaches classified for blending elements, all with differing applicability depending on the general model used, along with choices of element types and enrichments. Four types of classifications can be recognized as general approaches to solve the issue of blending elements:

i) Corrected/Weighted XFEM
ii) Patch-based enrichments
iii) Hierarchical shape functions in blending elements
iv) Assumed strain blending elements
v) Shifted step-enrichments

Corrected/Weighted XFEM

Corrected/Weighted XFEM is an approach that localizes the enrichment approximation further by adding the contribution of a ramp function $R(x)$ constructed by FE shape functions of the form:

$$R(x) = \sum_{i \epsilon I} N_i^*(x) \tag{28}$$

in the approximation Equation (25) by multiplication to the enrichment term, which then becomes:

$$u^h(x) = \sum_{i \epsilon I} N_i(x) u_i + \sum_{i \epsilon I^*} N_i^*(x) \cdot R(x) \cdot \psi(x) a_i \tag{29}$$

Then, the modified enrichment term is non-zero only in the reproducing and blending elements. Consequently, N_i^* is a partition of unity in both the reproducing and blending elements, which enables the modified enrichment function to be reproduced exactly wherever the function is non-zero. Thus, no effect associated with blending elements arises. [22, 14]

Patch-based enrichments

The problem of blending elements is avoided by suppressing them altogether by decomposing the computational domain into regions where all nodes are either enriched or approximated with standard FE, as seen in Figure 2-22. Consequently, no blending elements exists with this approach, and the regions are instead needed to be point-wise coupled at the nodes to enforce continuity across the boundaries, which can be done with additional constraints such as Lagrange multipliers or adding penalty terms to the approximation. [17, 14]

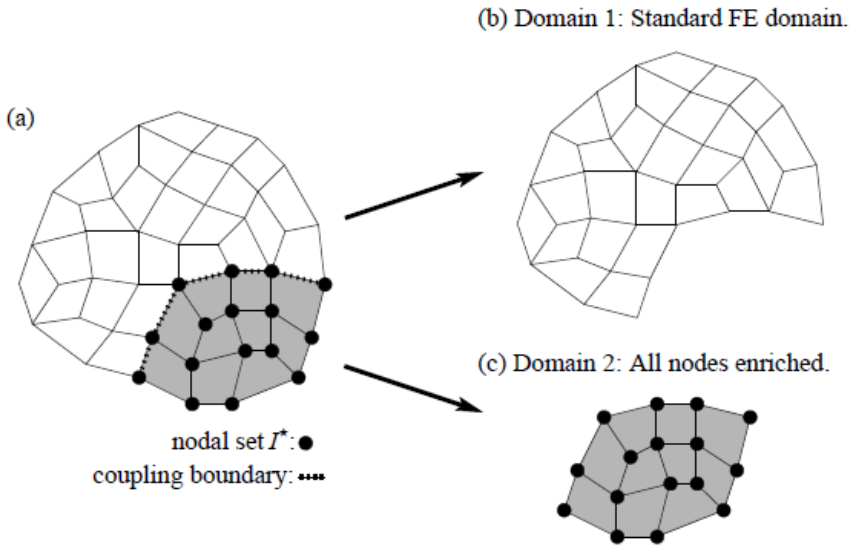

Figure 2-22: The complete computational domain a), is subdivided into, b) a standard FE domain, and c) a fully enriched domain to suppress the issue of blending elements [14]

Hierarchical shape functions in blending elements

As the enrichments are of polynomial behavior, it is proposed by Chessa et al [16] and Tarancón et al [21] that the effect of the blending elements and any unwanted terms can be compensated for by introducing additional higher order hierarchical shape functions to the partial enrichment. However, the cancellation of the errors may not be complete with any arbitrary enrichment function, which is a limitation. The approach subsequently adds additional degrees of freedom and has been proposed for linear triangular as well as higher order elements, however results may not consistently be optimal.

Assumed Strain blending elements (AS method)

This approximation is suggested for general enrichment functions and proposes a solution to eliminate the unwanted terms produced by partial enrichments, by introducing enhanced strain fields in the blending elements. For such a procedure the exact form of the unwanted terms is required, which causes the correction of the enhanced strain fields to be element and enrichment dependent. The drawback of this approach is therefore the difficulties in constructing the functions for the correction and AS approximation itself. [16, 17]

Shifted step-enrichments

With the use of a step function, such as the sign enrichment function, the effect of shifting the enrichment function on the standard FE shape functions across a discontinuity can be seen in Figure 2-23, as compared to Figure 2-20. The direct result of shifting the sign enrichment limits the effect of the enrichment to the reproducing element, which contains the discontinuity.

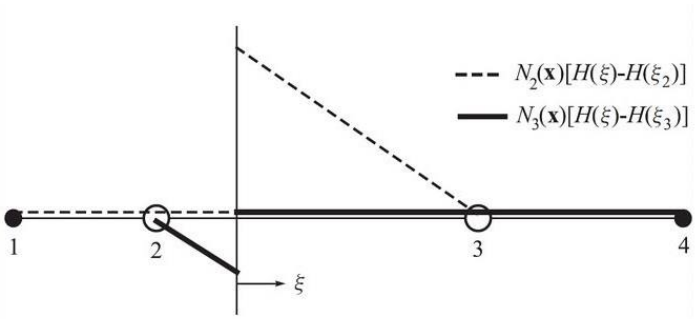

Figure 2-23: Effect of shifting the sign function on the shape functions for enriched nodes 2 and 3 containing a discontinuity [4]

As a result, with step enrichments the blending elements remains at constant value and when introducing a shifted approximation, the value disappears and becomes identically zero. Thus, there is no need for additional consideration for the blending elements, which is a significant beneficial aspect of step enriching and shifting the approximation. [4, 23]

2.4.2.4 Cohesive zone concept and traction-separation law

The concept of cohesive zone models has been utilized widely to evaluate stress singularities in linear elastic fracture mechanics (LEFM) and to approximate non-linear material separation behavior and evaluate various material failures. In general, LEFM is characterized by traction-free surfaces and is only applicable when the fracture process zone, i.e. the zone around the crack tip, is assumed to be "small". However, when that is not the case, other models need to be considered. In conjunction with XFEM, cohesive models enable crack interfaces to include traction and allows any nonlinear behavior to be modeled explicitly. [24, 25]

After crack initiation, with the introduction of a discontinuity across a ply, the interaction between the separated plies is expressed through an interface cohesive zone model. The tensile/compressive and shearing tractions at the interface are then calculated from the cohesive zone model, through a traction-separation law, which describes the evolution of the tractions in terms of normal and tangential displacement jumps. The separated plies are therefore coupled at the discontinuity depending on local relative displacement jumps governed by a cohesive traction-separation law. [26]

The traction-separation relationship is a fundamental aspect in cohesive zone modeling. It governs the stress/force-displacement across the discontinuity, which area under the curve represents the fracture energy dissipated, and the relation of which the cohesive traction generally decreases to zero. With a decrease in cohesive traction during separation, a global stiffness softening of the loaded material occurs. Subsequently, cohesive zone models take into account the gradual transition from full to zero material strength. In general, the shapes of such softening condition can be described by several interface laws, such as: linear, bi-linear, exponential, trapezoidal, linear-parabolic etc. as can be seen in Figure 2-24: Examples of interface law with a) a linear and b) an exponential softening . Based on a study of pure mode cases, Alfano [27] suggests the exponential law to be optimal in terms of FE approximations, while bi-linear law provides fairly accurate results with less computational efforts.

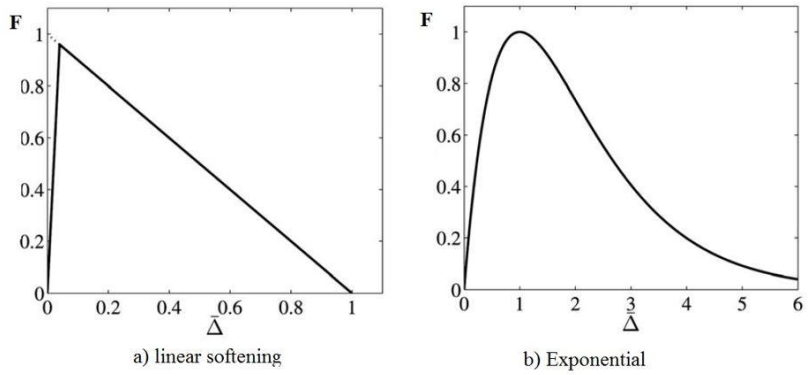

Figure 2-24: Examples of interface law with a) a linear and b) an exponential softening [24]

In the existence of a crack in the domain, the FE approximation of nodal displacements and test functions are split into continuous and discontinuous degrees of freedom, where the discontinuous degrees of freedom are enriched with a traction contribution, in compliance with Equation (25). For the internal forces of such an approximation and partition, is then:

$$f^{int} = \begin{Bmatrix} f_{cont}^{int} \\ f_{disc}^{int} + f_{traction} \end{Bmatrix} = \begin{cases} \int_A \boldsymbol{B}^{c^T} \boldsymbol{\sigma}\, dA = 0 \\ \int_A \boldsymbol{B}^{d^T} \boldsymbol{\sigma}\, dA + \int_\Gamma 2\, \bar{\boldsymbol{N}}\, \boldsymbol{t}\, d\Gamma \end{cases} \tag{30}$$

where the internal continuous forces are represented as in classical FE approximation over the area A in the 2D case, with $\boldsymbol{B}$ as the derivative of the shape functions and $\boldsymbol{\sigma}$ as the internal stresses/forces. However, for the discontinuous partition, the internal forces are enriched with the contribution of an additional $f_{traction}$ term over a crack surface Γ with the traction $\boldsymbol{t}$, that depends on the displacement jump according to the choice of traction-separation law.

Similarly, the constitutive relation of the domain, represented by a global stiffness matrix, is partitioned and an additional stiffness contribution dependent on the cohesive zone model is added into the discontinuity, as the following:

$$K_{Global} = \begin{bmatrix} K_{cc} & K_{cd} \\ K_{dc} & K_{dd} + K_{traction} \end{bmatrix} \tag{31}$$

whereas in general, $K_{Global} * a_{nodal\ displacement} = f$, and the cohesive zone model alters the stiffness and the internal forces of the domain depending on the nodal displacements, following the traction-separation law and the stiffness degradation through softening and damage evolution laws. [28]

3 Methodology

The modeling of matrix cracks in FRP laminates under transverse compression is implemented through two approaches: smeared crack approach and XFEM. The material model used is developed by Gutkin & Pinho in [7], in which damage is coupled with friction acting on the crack surfaces. This chapter describes the detailed framework of the models and the processes used to approach the numerical modeling of discontinuities and the step-wise implementation of loading cases and numerical schemes.

3.1 Framework of the models

It can be assumed that a FRP ply behaves transversally isotropic and linear elastic when it is intact. Therefore, the stress-strain relation can be described by the constitutive matrix as in Equation (12). However, this is not valid any longer upon damage initiation. Hence, a new constitutive relation is needed to capture the material stiffness softening, which will be discussed further in the following sections.

For the case of interest in this thesis, considering the loading condition and the trivial value of the thicknesses of the plies in comparison with the other dimensions of the model, the strain in the fiber direction can be neglected and assuming plane-strain condition is not a compromising assumption. Also, it is assumed that the damage is developed throughout the structure width, therefore, only a cross section of the structure can be modeled to save computational efforts. Figure 3-1 illustrates the actual 3D case and the simplified 2D case, which will be considered in the rest of study.

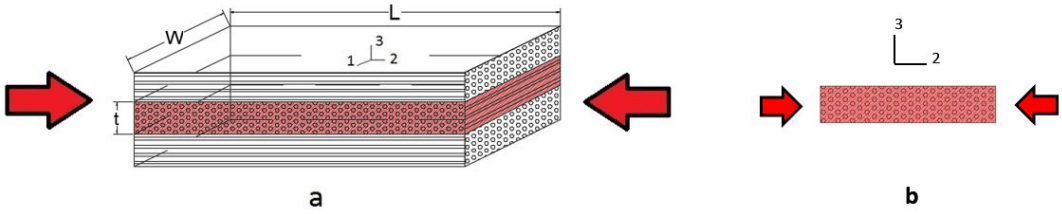

Figure 3-1: a) the loaded FRP laminate with the middle ply under transverse compression, b) simplified model in 2D

Fixed crack modeling

Upon damage initiation, it is assumed that a planar equivalent crack with fixed orientation is generated in the damaged area of the material. The assumption is physically reasonable since the crack propagation in a very thin ply is not of interest and computationally efficient due to the fact that the crack orientation is not evaluated at every loading step.

The stresses and strains on the crack plane can be computed by transformation of the global stresses and strains into the local ones complying with the local coordinate system aligned with the fracture plane, as is shown in Figure 2-5. As a result, the traction vector on the crack plane is computed, and then, the constitutive law including the damage and friction is constructed to enable the calculation for the cohesive traction

on the crack interface. This cohesive traction is then used to resolve back into the global stress, and consequently, the global strains can be computed.

Transformation from global to local coordinates

The transformation of the stresses and strains between global and local coordinates is conducted by means of a transformation matrix as defined in Equation (6). As a result, the local stresses and strains can be computed as in Equation (5). Further, the traction vector and the corresponding strain vector in plane strain condition are then defined as:

$$\begin{aligned} \boldsymbol{\sigma^{nt}} \cdot \mathbf{n} &= (\ \sigma_n \quad \tau_t\ )^T \\ \boldsymbol{\varepsilon^{nt}} \cdot \mathbf{n} &= (\varepsilon_n \quad \gamma_t\ )^T \end{aligned} \tag{32}$$

where $\boldsymbol{\sigma^{nt}}$ and $\boldsymbol{\varepsilon^{nt}}$ are 2×2 stress and strain matrices respectively, and $\mathbf{n} = (1 \quad 0)^T$ in the local 2D coordinate system.

Damage initiation criterion

The failure mode for a matrix under transverse compression is the sliding failure mode dominated by shear stresses. Therefore, only the shearing component of the traction computed in Equation (32) is used in the damage initiation criterion, which is defined as:

$$f(\alpha) = \max_{\alpha \epsilon [0, \frac{\pi}{2}]} \left| \frac{\tau_t}{S_t} \right| \tag{33}$$

where S_t is the shear strength of the material. The fracture initiation factor f is calculated for a range of possible fracture angles α, where the crack initiates once the shear stress reaches S_t and the fracture plane angle corresponds to the angle in which f is maximum. Furthermore, the stress-strain relation does no longer follow Hooke's law and is described by Equation (4) instead, where d only affects the tangential stiffness G in the current work, as the cracks are closed under compression and do not degrade the material normal stiffness.

Damage evolution

Upon damage initiation, the damage variable is computed as a function of the shear strains γ_t as:

$$d = 1 - \frac{\gamma_0}{\gamma_t} \left(\frac{\gamma_f - \gamma_t}{\gamma_f - \gamma_0} \right) \tag{34}$$

where γ_0 corresponds to the shear strain at damage initiation and γ_f is the shear strain at the fracture point and is calculated in the similar way as in Equation (18), where for the sliding failure mode (mode II), is justified as:

$$\gamma_f = 2\frac{(G_{IIc}/l_c)}{\tau_0} \tag{35}$$

where l_c is the characteristic length computed as in Equation (19) to adjust the fracture energy to the element size and the angle of the fracture plane.

Combining damage and friction

Usually, micro-cracks generated under tensile loading are assumed to be traction free. However, under compression the cracks are closed and able to carry load. In this thesis, the frictional effects due to the sliding of the interfaces of the closed cracks are also taken into account as proposed by Gutkin & Pinho in [7]. Therefore, the model is described as:

$$\boldsymbol{\sigma^{nt}} = \begin{bmatrix} \sigma_n \\ (1-d)\tau_t \end{bmatrix} + \begin{bmatrix} 0 \\ d \cdot \tau^{friction} \end{bmatrix} \tag{36}$$

where d is the damage variable. It is worth mentioning that in this model, for a fully damaged material $d = 1$, only the friction term remains. The friction term for the sliding case can be expressed based on Coulomb law as:

$$\tau^{friction} = \begin{cases} G(\gamma - \gamma_s) & without\ sliding \\ -\mu\sigma_n & with\ sliding \end{cases} \tag{37}$$

where γ_s is the sliding shear strain, γ is the total shear strain, μ is the friction coefficient in sliding direction, and the contact stiffness in sliding direction is assumed to be similar as the shear modulus G.

Sliding criterion

To identify the sliding initiation, a sliding criterion ϕ is defined as:

$$\phi = \left\|\tau^{friction}\right\| + \mu(\sigma_n - p_0) \tag{38}$$

where p_0 is introduced to take into account the internal pressure e.g. residual stresses, and sliding occurs if ϕ is greater than zero.

Upon sliding, the sliding strain γ_s is altered by the sliding increment and computed as follows:

$$\dot{\gamma_s} = \dot{\lambda} \frac{\partial \phi}{\partial \tau^{friction}} = \dot{\lambda} \tag{39}$$

with $$\dot{\lambda} = \left(\frac{\phi}{G}\right) \tag{40}$$

Finite element implementation

The FE implementation is done by integrating the global stresses incrementally over a sequence of time steps with strain and displacement stepping for the smeared crack approach and the XFEM approach respectively. The global stresses are transferred to the local coordinates corresponding to a range of possible fracture planes to assess damage initiation in the material based on the selected damage initiation criterion. Upon damage initiation, a crack with the fixed orientation is assumed to be generated inside the material. Later the damage variable is computed and taken into account which results in a reduction in the material stiffness as well as the local stresses. Moreover, the tangential component of the stress is used to check for sliding, where in case of sliding, the frictional stresses need to be corrected. Finally, the local stresses are transferred back into the global stresses. The XFEM implementation, as a discrete method, utilizes the same procedure as above-mentioned. However, instead of strains to drive damage growth, relative discontinuity jumps are considered at the crack shearing direction through a cohesive zone model using a traction-separation law.

The implemented algorithm is presented briefly as:

1. Initial conditions

$$(\boldsymbol{\varepsilon_n}, \Delta\boldsymbol{\varepsilon_{n+1}}, f_n, d_n, \gamma_{s,n}) \tag{41}$$

2. Update strain and stress predictor

$$\begin{aligned} \boldsymbol{\varepsilon_{n+1}} &= \boldsymbol{\varepsilon_n} + \Delta\boldsymbol{\varepsilon_{n+1}} \\ \boldsymbol{\sigma_{n+1}} &= \mathbf{C} \cdot \boldsymbol{\varepsilon_{n+1}} \end{aligned} \tag{42}$$

3. Failure index and check damage initiation

$$\boldsymbol{\sigma}_{\boldsymbol{n+1}}^{\boldsymbol{nt}} \cdot \mathbf{n} = (\mathbf{T} \cdot \boldsymbol{\sigma}_{\mathbf{n+1}}^{\mathbf{xy}}) \cdot \mathbf{n}$$
$$f_{n+1}(\alpha) = \max_{\alpha \epsilon [0, \frac{\pi}{2}]} \left| \frac{\tau_t}{S_t} \right| \quad , \ \alpha \epsilon \, [0\,;90]$$
$$f_{n+1} = \begin{cases} f_n & \text{if} \quad f_{n+1} \leq f_n \\ f_{n+1} & \text{if} \quad f_{n+1} > f_n \\ 1 & \text{if} \quad f_{n+1} \geq 1 \end{cases} \tag{43}$$

4. Damage variable and corrector

$$d = 1 - \frac{\gamma_0}{\gamma_{t,n+1}} \left(\frac{\gamma_f - \gamma_{t,n+1}}{\gamma_f - \gamma_0} \right)$$
$$d_{n+1} = \begin{cases} d_n & \text{if} \quad d_{n+1} \leq d_n \\ d_{n+1} & \text{if} \quad d_{n+1} > d_n \\ 1 & \text{if} \quad d_{n+1} \geq 1 \end{cases} \tag{44}$$
$$\boldsymbol{\sigma}_{\boldsymbol{n+1}}^{\boldsymbol{nt}} = \mathbf{K}\, \boldsymbol{\varepsilon}_{\mathbf{n+1}}^{\mathbf{xy}}$$
$$\text{with } \mathbf{K} = \begin{bmatrix} E & 0 \\ 0 & (1-d)G \end{bmatrix}$$

5. Frictional stress prediction

$$\tau_{n+1}^{friction} = G(\gamma_{n+1} - \gamma_{s,n}) \tag{45}$$

6. Check sliding

$$\phi = \left\| \tau^{friction} \right\| + \mu(\sigma_n - p_0) \tag{46}$$

7. Frictional stress corrector

$$\dot{\lambda} = \left(\frac{\phi}{G} \right)$$
$$\varepsilon_{s,n+1} = \varepsilon_{s,n} + \dot{\lambda}_{n+1} \Delta t$$
$$\tau_{friction} = -\mu(\sigma_n - p_0) \tag{47}$$
$$\boldsymbol{\sigma}_{\boldsymbol{n+1}}^{\boldsymbol{nt}} = \boldsymbol{\sigma}_{\boldsymbol{n+1}}^{\boldsymbol{nt}} + \begin{bmatrix} 0 \\ d_{n+1} \tau_{n+1}^{friction} \end{bmatrix}$$

8. Return stress to the global axis as in (6).

Material properties

The material properties used in the current study are the same as the material properties tested in Swerea/SICOMP. These properties are listed in Table 1. [7]

Table 1: Material properties of T700/MTM57

Longitudinal elastic modulus	$E_{11}\ [GPa]$	128
Transverse elastic modulus	$E_{22}\ [GPa]$	7.9
Shearing modulus	$G_{12}\ [GPa]$	3
Poisson's ratios	ν_{12}	0.3
Poisson's ratios	ν_{23}	0.4
Fracture Toughness of the material	$G_{IIc}\ [KJ/m^2]$	2
Internal pressure in transverse direction	$P_{Ot}\ [MPa]$	30
Shear strengths	$S_t\ [MPa]$	60
Friction coefficient	μ_t	0.3
Density	$[Kg/mm^3]$	1.6 e-6

3.2 Smeared crack model implementation in Abaqus/Explicit

There are three main analysis products in Abaqus such as Abaqus/Standard, Abaqus/Explicit, and Abaqus/CFD. Abaqus/Standard solves the problems implicitly and is used for a wide range of problems of any type. For quasi-static cases, Abaqus/standard is usually used for the problems including time-dependent material properties e.g. creep. However, Abaqus/Explicit solves the problems explicitly and is able to solve quasi-static problems as well as dynamic problems. It solves the problems with very small time increments without solving the coupled system of equations in each increment. For large models, it requires less system resources in comparison with Abaqus/Standard and is more efficient in highly non-linear problems. Finally, Abaqus/CFD is used to computationally solve the fluid dynamic related problems. [29] Considering the above mentioned descriptions and underlying assumptions for the case of interest in the current work, Abaqus/Explicit is selected to be used. In the following sections the procedures to set up the models in Abaqus/Explicit are explained.

Conventionally, the smeared crack model has been utilized to capture matrix cracks effects on the material stiffness. A case is modeled within Abaqus/Explicit based on the framework presented in Section 3.1. To do so, the subroutine developed by Swerea/SICOMP is used as the solver to take into accounts both friction and the damage. A mesh study is carried out for three different mesh sizes for two cases, where in one case the damage is combined with the friction and in the other case the friction is neglected. Furthermore, an element type study is conducted to evaluate which element type is the most compatible with the smeared crack approach.

3.2.1 Model setup

To setup a model in Abaqus the following standard steps need to be taken:

- Create the part and assign the material parameters
- Define the loading steps and analysis type
- Define loads and boundary conditions
- Mesh the model
- Solve for the sought results

Geometry and property

The first step of modeling is creating the geometry of the part. Considering the loading condition, fibers direction, and physical dimensions of the specimen, it can be assumed that plane-strain condition is valid for the model and the material is assumed transversally isotropic i.e. $E_{22} = E_{33}$. Therefore, a 3D, deformable, homogenous solid part under plane-strain condition is created. Furthermore, in order to reduce the influence of the supports on the damage initiation position and to be able to capture the crack angle properly, the part is designed as a rectangular cube as is shown in Figure 3-2. However, to avoid buckling instability problems, the length of the part is designed to be at most three times higher than the thickness of each ply i.e. the in-plane dimensions of the part are defined as $L = 0.6\ mm, t = 0.2\ mm$.

Note that in this model fibers are aligned with the axis 1 of the local coordinate system and X axis of the global coordinate system.

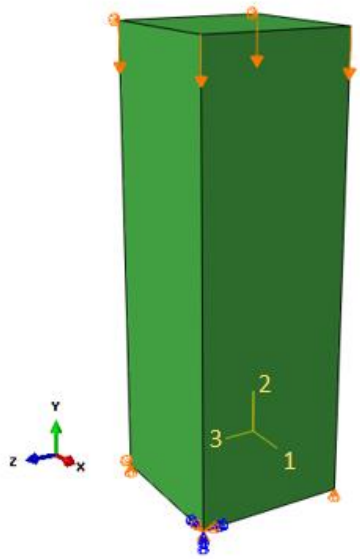

Figure 3-2: Created part in Abaqus including the boundary conditions, global coordinate system XYZ and local coordinate system 123

The assigned material properties to the created geometry are the same material properties as listed in Table 1.

Step

Analysis type and related parameters are defined in the module step. In this specific case, explicit dynamic excluding non-linear geometry effects (NLGEOM OFF) is selected. The number of time increments for the analysis is selected large enough in order to keep the inertial effects negligible and the simulation quasi-static, to have a fair comparison with the XFEM simulation. Also, the analysis field outputs such as forces, displacements, etc. and history outputs such as artificial, kinetic, and strain energies, etc. are requested to be recorded during the analysis for post processing consideration and assessment of the assumed assumptions trueness.

Loads and boundary conditions

The displacements in Y direction on the bottom face of the model are prevented, and the upper face is subjected to the prescribed uniform displacement in the $-Y$ direction. Also all degrees of freedom for one of the corners on the bottom face are locked to avoid rigid body motions of the model during the simulation, and the degrees of freedom for the nodes on the back face of the part are locked in X direction to keep the model in-plane during the loading process, see Figure 3-2.

Mesh

The created part is meshed by 8-node linear brick continuum elements with reduced integration points named as C3D8R, as Gutkin & Pinho in [7] applied this element in their finite element model. This element suits the uniform shape of the created geometry, and has better convergence rate and less sensitivity of brick/quadrilateral elements in regular meshes than triangular elements to the mesh orientation. Also the first order triangular elements are so stiff and mesh needs to be very fine to achieve acceptable accuracy [29].

In conjunction with XFEM, for comparison purposes, a mesh study is conducted by three different mesh sizes. At first, the model is analyzed with one element per ply thickness i.e. $l_{elem} = 0.2\ mm$. In this case a cubic element is used to avoid buckling instability problems. Furthermore, the models with 4 and 6 elements per ply with element size of 0.05 and $0.033\ mm$ respectively are considered, see Figure 3-3.

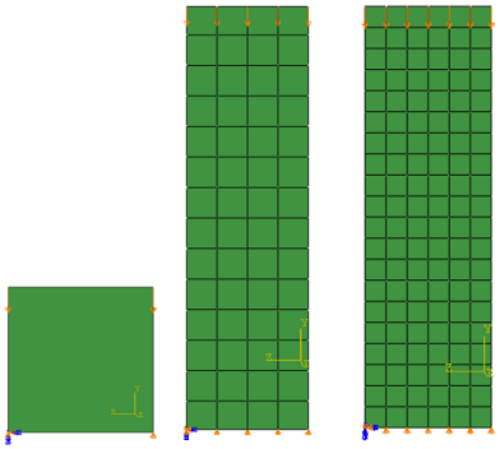

Figure 3-3: Models with a) 1 element, b) 4 element, c) 6 element through the thickness

Solver

In the module job, one can choose to use Abaqus built in solvers or introduce a self-developed subroutine file as a solver for specific solutions. In this thesis, the material model developed and implemented by Swerea/SICOMP in a FORTRAN user subroutine is used to combine the damage with friction and capture stiffness softening based on the bi-linear cohesive law as described in Section 2.2.

3.2.2 Validation

In order to validate Abaqus simulation results for the model of interest in this thesis, artificial energy and hourglassing, kinetic energy and dynamic effects for all mesh sizes are monitored.

Artificial energy and hourglassing

Artificial energy is an unreal energy that is required to keep the shape of the elements physically reasonable and avoid hourglassing during the simulation. In general, hourglassing may occur in the models with linear 3D solid elements with reduced integration points such as C3D8R. Since they have only one integration point, they may deform in such a way that the strain of the element remains zero, as can be seen in Figure 3-5, where none of the dotted lines are elongated or tilted while the element is deformed. As a consequence, all the stress components in this element are zero and the computed strain energy for such a deformation can be zero, and this causes error in the stress-strain diagram. One way of diagnosis of hourglassing is to look at the ratio between the artificial energy and the strain energy curve. For a reliable analysis, this ratio should not exceed 5%.

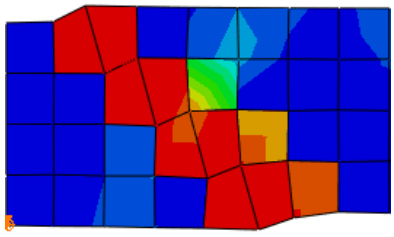

Figure 3-4: A deformed mesh with hourglassing

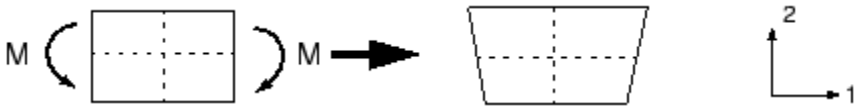

Figure 3-5: Deformed and undeformed linear element with reduced integration points in bending [29]

There are different treatments to reduce or remove hourglassing such as mesh refinement and distributing the point loads and boundary conditions on more number of nodes, using fully integrated elements instead of reduced ones, and adding artificial stiffness to the hourglassed elements in static or quasi-static problems. One way of adding artificial stiffness is to use enhanced hourglass control C3D8R elements, in which the stiffness coefficients are based on the enhanced strain method. [29] These elements give more accurate stress-strain results and typically generate stiffer responses in comparison with the default hourglass controlled elements.

To evaluate the effectiveness of the smeared crack approach, an element type study is conducted. Therefore, the problem is modeled with enhanced hourglass controlled and the default hourglass controlled C3D8R elements with one integration point and fully integrated elements C3D8I consisting of 8 integration points. The results are presented in Section 3.3.

Kinetic energy and dynamic effects

The kinetic energy for the model throughout the simulation is monitored and must be less than 10% of the strain energy in order to satisfy the quasi-static assumption [7].

Mesh study

A mesh study for different mesh sizes with one and more elements through the ply thickness is done to investigate the effect of mesh refinement in testing the limit of the smeared crack approach in comparison to the XFEM approach. For each case, the normal stress-strain curve together with the artificial energy-strain energy ratio are plotted and considered. To do so, the reaction forces on the top face nodes are summed up and divided by the area subjected to the load.

3.3 XFEM implementation in MATLAB

The case study of a matrix cracking in a unidirectional FRP ply under transverse compression is implemented in 2D using MATLAB. In order to apply a cohesive traction-separation law with XFEM, the previous framework described in Section 3.1 is reformulated, where the traction evolution is defined in terms of normal and tangential displacement jumps, rather than strains.

3.3.1 XFEM scheme/model

The local enrichment XFEM scheme utilized in this thesis includes the following:

- **Shifted sign function for enrichment terms to simulate strong discontinuities**, where the apparent difficulties with blending elements in discrete models, as described previously in Section 2.4.2.3, vanishes with this choice of approach, as no extra consideration has to be employed.

- **Non-linear cohesive traction model**, based on Gutkin & Pinho in [7], for compressive matrix cracking coupling damage and friction, with friction as the key contributor of the non-linear response.

- **Traction-separation law with linear softening**, in compliance with the non-linear cohesive traction model, to describe progressive damage to predict the failure of the ply structure.

- **Fixed crack model**, where once the discontinuity and crack angle are identified and implemented, they remain fixed and the plane of orientation do not change.

- **Numerical integration**, the elements of choice are squares with quadrilateral subdomains for elements containing discontinuities, with the order of 2x2 Gauss integration points. Likewise, for the discontinuity line segments that cuts through the domain.

- **Newton's method**, as the choice of iteration scheme. For XFEM, this requires the linearization of the internal forces and the derivation of the cohesive tangent stiffness, expressed by the rate of change for the displacement jump in both

normal and tangential directions, to be later expressed and added to the residual out-of-balance force vector and the Jacobian stiffness matrix.

3.3.2 XFEM procedure

The XFEM implementation procedure entails the classical standard FE numerical implementations and additional necessary functions related to discontinuity modeling, damage evolution and traction-separation law.

The evaluation of the stresses in the domain is performed incrementally by stepping in a constant displacement for each time step. The constitutive behavior of the domain is assumed to follow Hooke's law with linear elastic and transversely isotropic behavior under the plane strain assumption.

To relate the damage evolution to the displacement jumps, the strains γ_0 and γ_f, are reformulated in relation to displacement jumps to δ_0 and δ_f instead, where the damage variable is then expressed by displacement jumps in both material properties and the updated value for the current time step.

The parameters k_N and k_T are material properties that represents the stiffness across the discontinuity in normal and transverse shearing directions. With the XFEM implementation, the stiffness of the coinciding interfaces is dependent on a traction-separation law, which in turn is expressed by the stiffness parameters of k_N and k_T. Thus, an increase in these parameters equals an increase in the total stiffness of the cohesive zone model, where converged stiffness's across the discontinuity are used in order to properly capture the crack shearing behavior.

The procedure of the XFEM implementation

1) The building of a constitutive matrix for the global domain that is able to include enriched degrees of freedom when a nodal subset of the domain is enriched.

2) Constructing and updating boundary conditions of the domain before and after damage initiation: When enriching the discontinuous elements additional degrees of freedom are added into the approximation space, which require adjustments after finding fracture plane.

3) Increment loading per time step to estimate local stress tensors and check for damage initiation by evaluating a chosen set of test angles consisting of 15° increments from 0° to 90°. Upon each time step, damage initiation is evaluated at the middle element as the crack is assumed to initiate at the middle of the domain.

4) Upon damage initiation, the description of the crack constructed through a level-set function, and a fixed-crack model is implemented with the angle that resulted in the highest failure index, following the damage initiation criterion in Equation (33).

5) Evaluate the damage variable according to Equation (34), but defined by the displacement jumps rather than strains, as the following:

$$d = 1 - \frac{\delta_0}{\delta_{t,n+1}}\left(\frac{\delta_f - \delta_{t,n+1}}{\delta_f - \delta_0}\right)$$
$$d_{n+1} = \begin{cases} d_n & \text{if} \quad d_{n+1} \leq d_n \\ d_{n+1} & \text{if} \quad d_{n+1} > d_n \\ 1 & \text{if} \quad d_{n+1} \geq 1 \end{cases} \tag{48}$$

where δ_t is the transverse discontinuous jump that drives the damage evolution, in conjunction with δ_0 and δ_f representing the discontinuous jump required for damage initiation and complete failure, respectively. Complete failure is achieved when $d = 1$.

6) Evaluate the traction based on linear softening traction-separation law and the current damage of the time step.

$$\mathbf{t}_{\boldsymbol{n+1}}^{\boldsymbol{nt}} = \mathbf{K}\,\boldsymbol{\delta}_{\mathbf{n+1}}^{\mathbf{nt}}$$
$$\mathbf{K} = \begin{bmatrix} k_N & 0 \\ 0 & (1-d)k_T \end{bmatrix} \tag{49}$$

7) Evaluate predictor for frictional stress similar, to Equation (45):

$$\tau^{friction} = (1-d)k_T(\delta_T - \delta_S) \tag{50}$$

8) Check for sliding with the following criterion:

$$\phi_{n+1} = \|\tau^{friction}\| + \mu(k_N\delta_N - p_0) \tag{51}$$

9) Frictional stress corrector: If sliding occurs, correct the frictional contributions in traction and cohesive tangent stiffness. Update the sliding displacement jump δ_s after convergence for current time step, and use as input for the frictional stress predictor in next time step.

$$\begin{aligned} \dot{\lambda} &= \left(\frac{\phi_{n+1}}{k_T}\right) \\ \delta_{s,n+1} &= \delta_{s,n} + \dot{\lambda}_{n+1}\Delta t \\ \tau_{friction} &= -\mu(k_N\delta_N - p_0) \\ \mathbf{t_{n+1}^{nt}} &= \mathbf{t_{n+1}^{nt}} + \begin{bmatrix} 0 \\ d_{n+1}\tau_{n+1}^{friction} \end{bmatrix} \end{aligned} \tag{52}$$

10) Transform using Equation (5) and return the tractions and cohesive tangent stiffness to the Newton iteration scheme.

4 Results

4.1 Smeared crack approach results

Stress-strain (S-E) curve for the model with one linear 3D solid element with reduced integration points (C3D8R) excluding non-linear geometry effects per ply thickness is presented in Figure 4-1. The orange curve represents the case with combined damage with friction and the blue curve corresponds to the frictionless case (indicated by "NoFr" suffix), which represents a linear stiffness softening as expected. It can be seen that the combined damage with friction case experiences a higher maximum stress level and dissipates more energy until final fracture, in comparison with frictionless case. Also, for the case where damage and friction are combined, the cracks are no longer traction free. Thus, a fully damaged element still can carry stress equivalent to the frictional stress on the crack interfaces.

To assess the validity of the simulations, the artificial energy over the strain energy (AE/SE) curves are also plotted in Figure 4-1. However, they remain zero through the entire simulations since there is no hourglassing effect, and consequently, no rise in artificial energy.

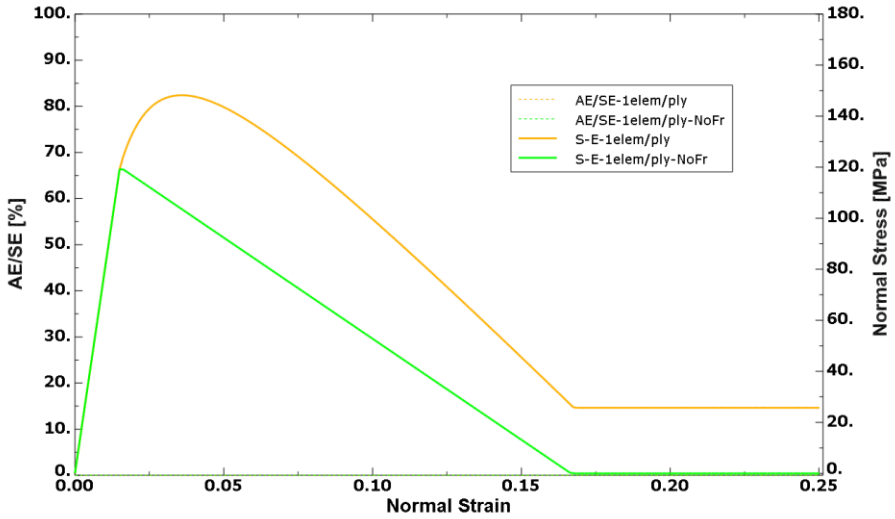

Figure 4-1: Stress-strain and artificial energy over strain energy curves for the mesh with 1 element per ply for frictionless case and the case with combined damage and friction

The mesh deformation for the above mentioned cases is the same and shown in Figure 4-2. As can be seen, the mesh with one element per ply cannot represent the crack angle and the wedge shape of the fully damaged elements successfully. Thus, in order to represent these effects, the mesh needs to be refined and the crack needs to be resolved.

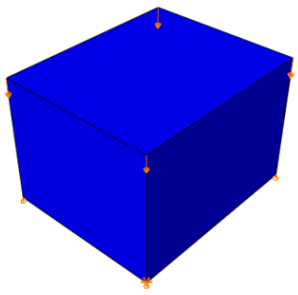

Figure 4-2: The deformation for the mesh with 1 element per ply for both frictionless and combined damage with friction cases

Figure 4-3 shows the S-E and AE/SE curves for the mesh with four C3D8R elements, excluding non-linear geometry effects, through the ply thickness for both the frictionless case and the case where damage and friction are combined. By having more elements per ply, hourglassing occurs in some elements and increases as the strain increase. Subsequently, the results become not reliable as AE/SE exceeds 5%. Since the cracks are assumed traction free in the frictionless case, the hourglassing increases much faster, which causes faster growth in artificial energy, and thus the results become unreliable in lower strain level in comparison to the other case.

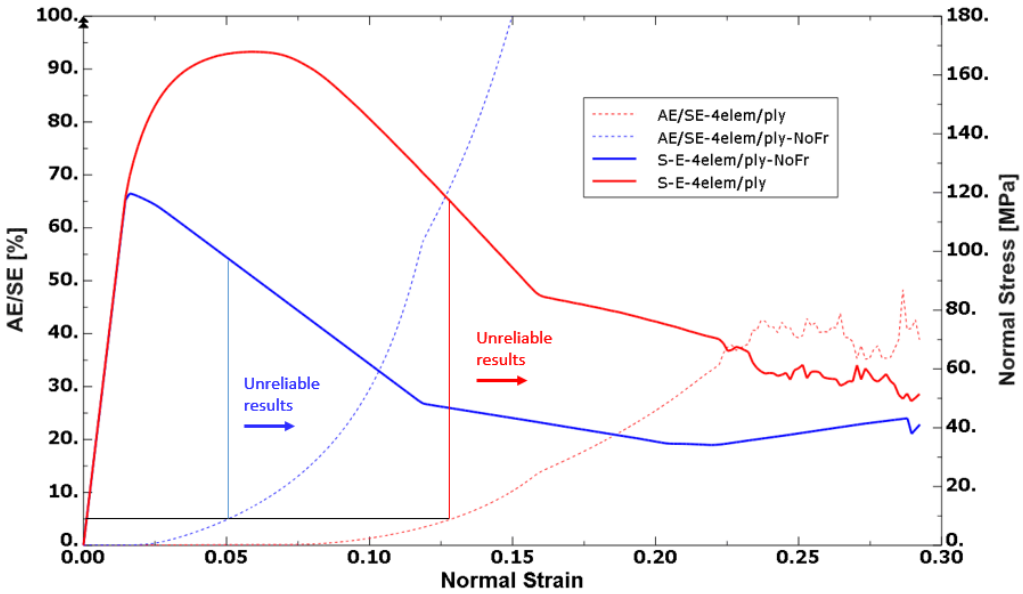

Figure 4-3: Stress-strain and artificial energy over strain energy curves for the mesh with 4 elements per ply for frictionless case and the case with combined damage and friction

The mesh deformations of the above mentioned cases are presented in Figure 4-4 where the intact and damaged elements are indicated by blue and red color respectively. It is worth noticing that the crack angle is effectively captured, however, still the mesh is not able to represent the wedge shape of the fully damaged elements correctly. Also note that, adding friction to the crack interfaces causes additional damage to the adjacent elements close to the crack band.

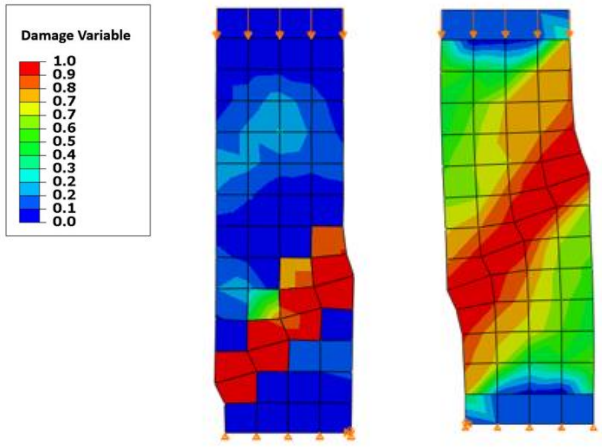

Figure 4-4: The deformation for the mesh with 4 elements per ply, the frictionless model (left) and the combined damage and friction model (right)

Figure 4-5 shows the S-E and AE/SE curves for the mesh with six C3D8R elements, excluding non-linear geometry effects, through the ply thickness for both the frictionless case and the case where damage and friction are combined. The corresponding deformations are presented in Figure 4-6. The same explanation as for the mesh with 4 elements per ply is also valid for the mesh with 6 elements per ply.

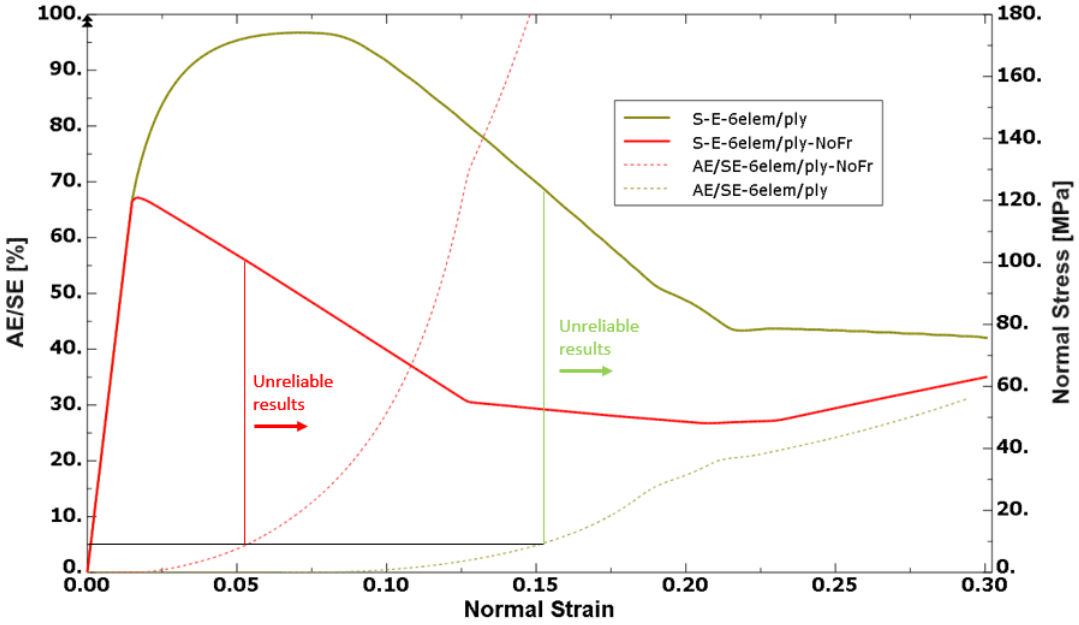

Figure 4-5: Stress-strain and artificial energy over strain energy curves for the mesh with 6 elements per ply for frictionless case and the case with combined damage and friction

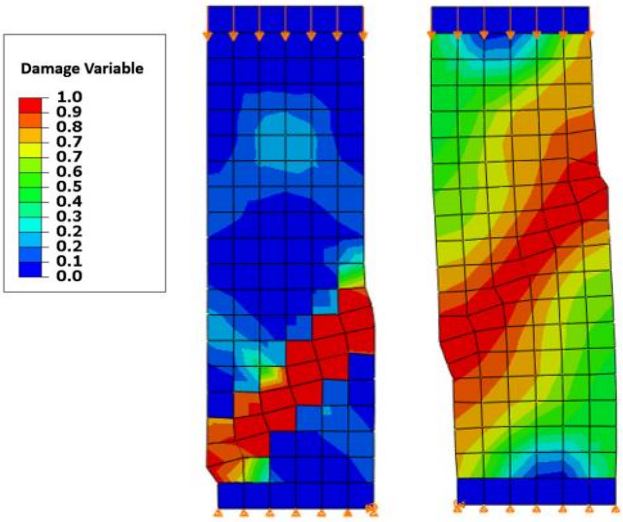

Figure 4-6: The deformation for the mesh with 6 elements per ply, the frictionless model (left) and the combined damage and friction model (right)

The S-E curves for both frictionless and the case with combined damage and friction for 3 different mesh sizes with C3D8R elements excluding non-linear geometry effects are gathered in Figure 4-7. As can be seen, the model with one element per ply can present the entire material response without any instability or oscillation, and the results are reliable since the artificial energy remains negligible for the entire simulation. However, the models with more than one elements per ply show non-smooth responses and the results become unreliable quite soon as the AE/SE exceeds 5%.

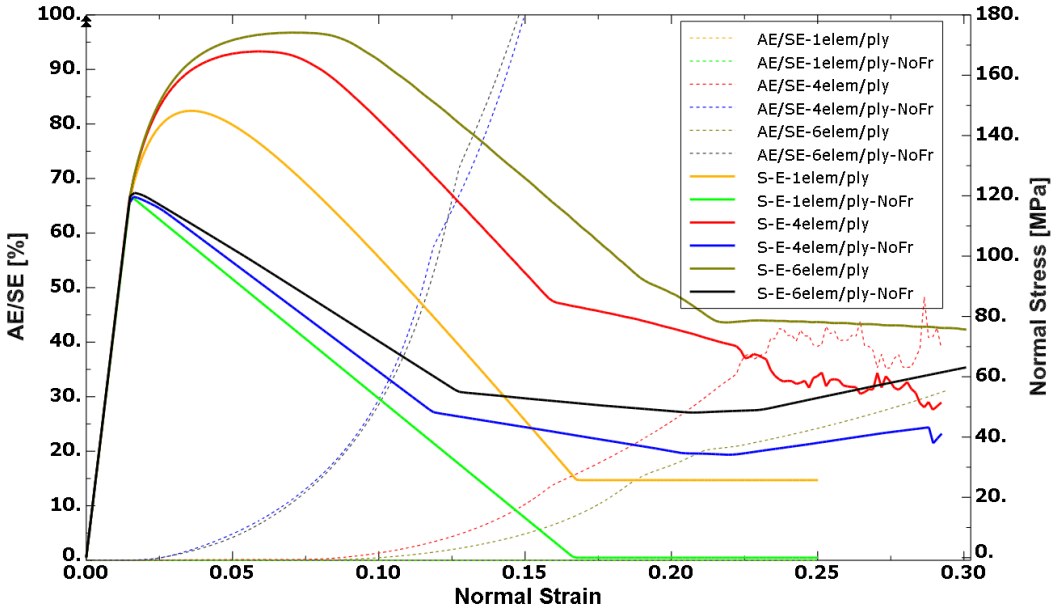

Figure 4-7: Stress-strain curves for the models with 1, 4, and 6 elements per ply for both frictionless case and the case with combined damage and friction

As can be seen from Figure 4-8, the S-E curve for the mesh with C3D8R elements almost coincides on the mesh with fully integrated elements C3D8I up to a certain strain level, where the AE/SE exceeds 5% for the model with C3D8R elements and the risk of shear locking occurrence is increasing in C3D8I elements. The mesh with C3D8R elements with enhanced hourglass control shows stiffer response, and the damage is distributed in more elements than the other cases. In other words, the strain localization is not well captured in this case. It is worth noticing that the artificial energy for the model with fully integrated elements C3D8I is zero throughout the simulation since these elements are not suffering from hourglassing as expected. The corresponding deformations are presented in Figure 4-9.

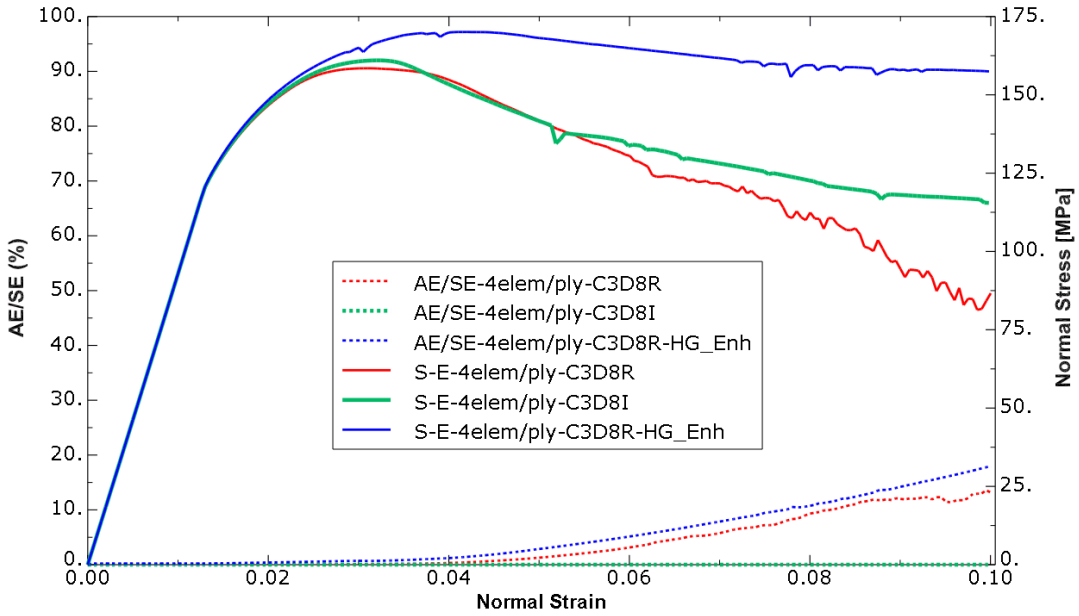

Figure 4-8: Stress-strain and artificial energy over strain energy curves for the mesh with 4 elements per ply

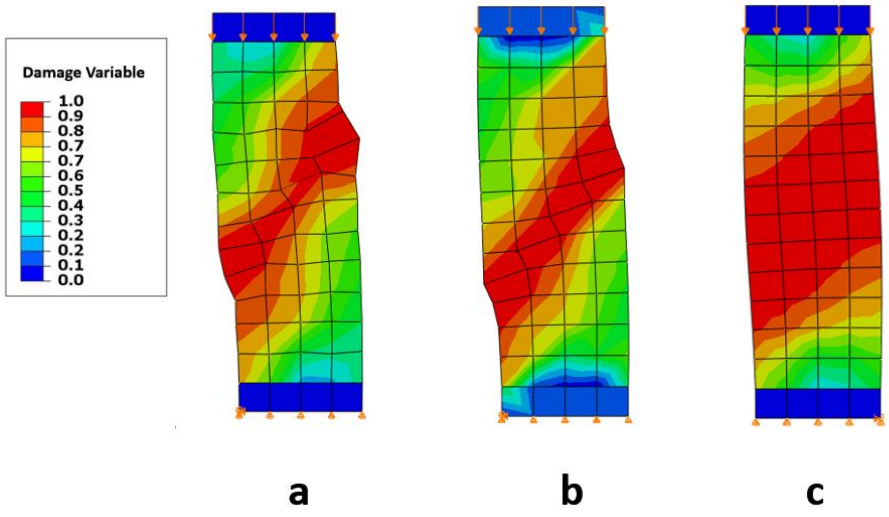

Figure 4-9: Deformation of the mesh with a) C3D8R, b) C3D8I, c) C3D8R with enhanced hourglass controlled

Figure 4-10 illustrates the S-E curves and AE/SE curves for the cases where damage is combined with friction and the mesh with six C3D8R elements excluding non-linear geometry effects per ply with and without element deletion existence. The S-E curve for the case with element deletion (the solid orange curve) corresponds to the case in which elements are not deleted during the simulation (the solid green curve) up to a certain strain level. For the case including the element deletion, a row of completely damaged elements is deleted at the strain level of 0.054, which physically causes global sliding initiation. As a result of element deletion, the artificial energy tends to remain negligible and the stress level drops dramatically. At the same strain level, for the case without element deletion existence, the increase of hourglassing in the damaged elements leads to a rise in artificial energy to keep the damaged elements in shape. As the strain increases higher artificial energy is needed, which results in AE/SE to exceed 5% and results become unreliable.

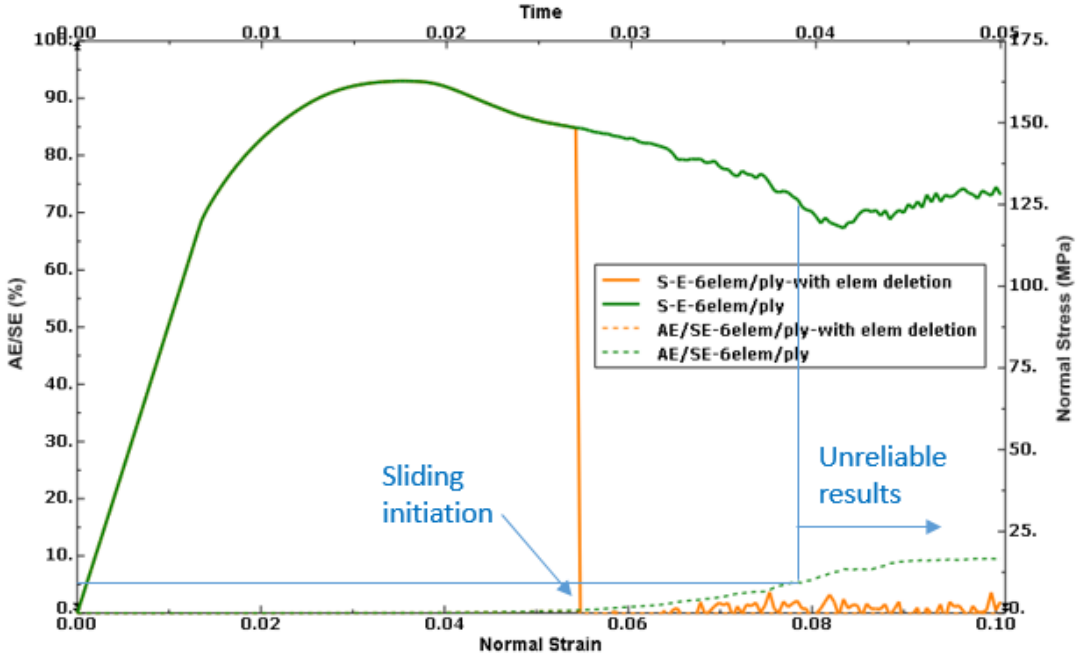

Figure 4-10: Stress-strain and artificial energy over strain energy curves for the cases with and without element deletion for the mesh with 6 elements per ply

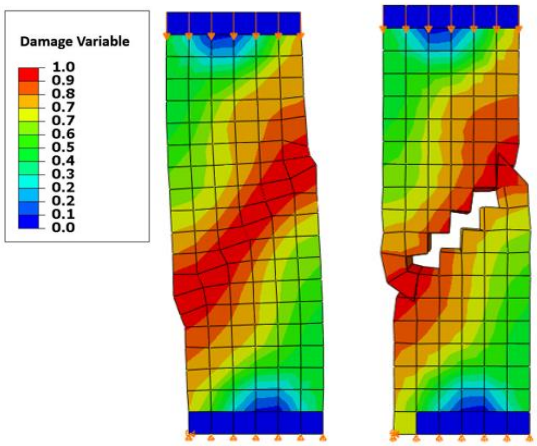

Figure 4-11: The deformation for the mesh with 6 elements per ply, No element deletion is included (left) and the case containing element deletion (right)

4.2 XFEM approach results

Figure 4-12 illustrates the results from the MATLAB simulation for the XFEM approach with one quadrilateral element per ply thickness, and the results from the Abaqus/Explicit simulation for the smeared crack approach, with one C3D8R element per ply thickness excluding non-linear geometry. The damage is initiated at the peak load based on the damage initiation criterion defined in Equation (43), where the stress at the fracture plane reaches the strength of the material for the corresponding failure mode. Note that the stress-strain curves of both approaches are identical. However, the damage in the XFEM approach is growing much faster than the smeared crack approach, and almost more than 60% of the material is damaged in the first increment after damage initiation.

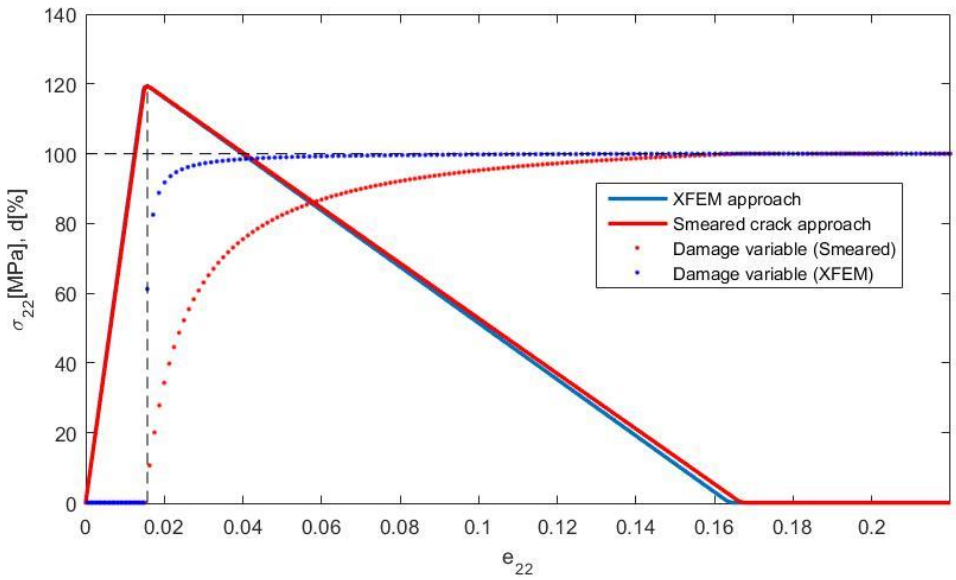

Figure 4-12: Stress-strain and damage evolution curves for the XFEM and the smeared crack approach for frictionless case with the mesh with 1 element per ply thickness

Figure 4-13 shows the results for the case where damage and friction are combined for the XFEM approach with one quadrilateral element per ply thickness, and the Abaqus/Explicit simulation for the smeared crack approach, with one C3D8R element per ply thickness excluding non-linear geometry. It is worth noticing the difference in the peak loads, damage evolutions, and the damage initiation point corresponding to the strain level equal to 0.015, where the material response starts to deviate from linear behavior due to the added frictional contribution on the crack interfaces.

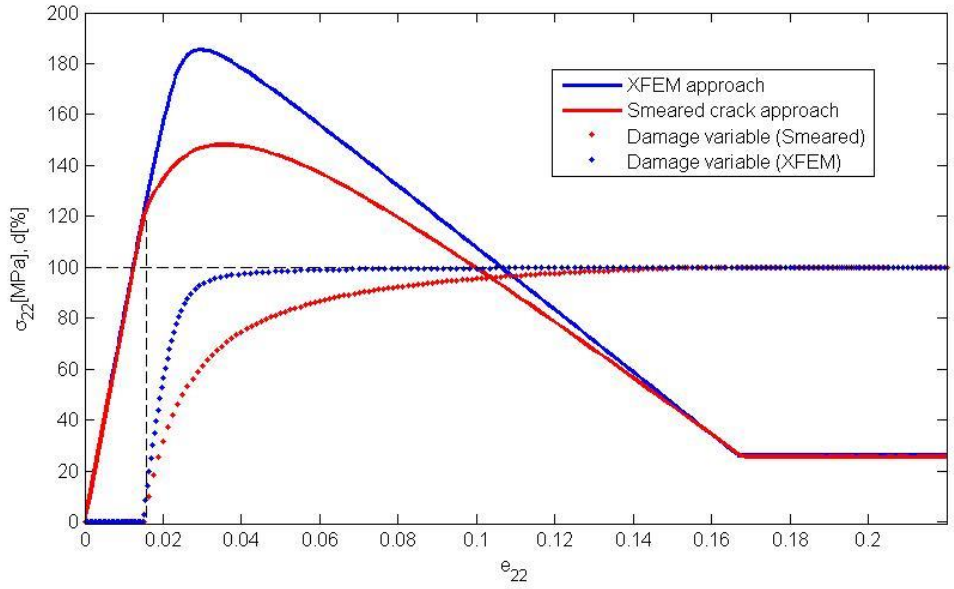

Figure 4-13: Stress-strain and damage evolution curves for the XFEM and the smeared crack approach for the combined damage and friction case with the mesh with 1 element per ply thickness

Results from a mesh study results for the XFEM approach for the frictionless case and the combined damage with friction case are plotted in Figure 4-14, Figure 4-15 respectively. As can be seen, the mesh convergence in the XFEM approach is successfully achieved for both cases.

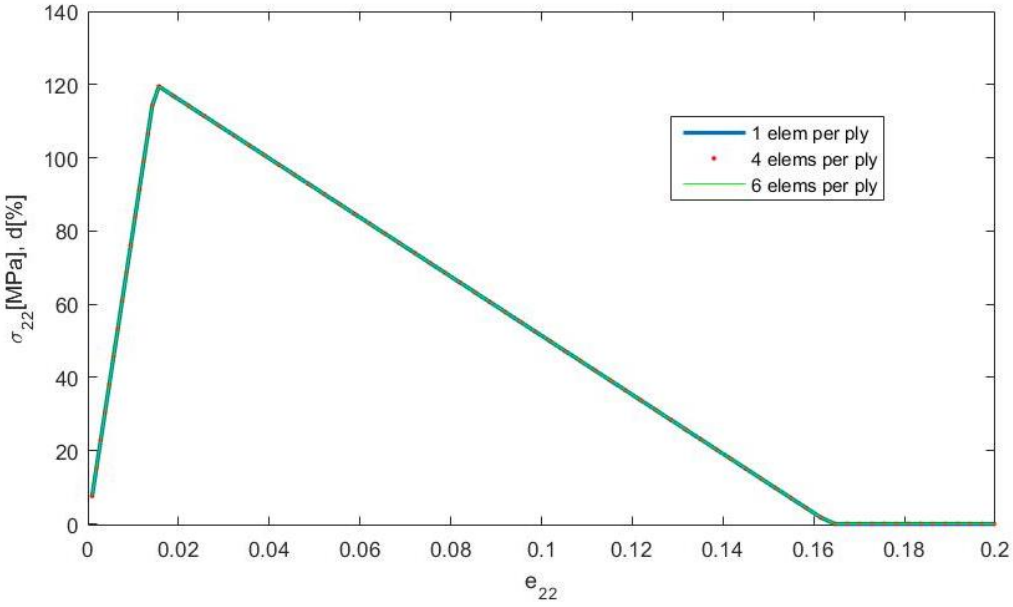

Figure 4-14: Mesh convergence for the XFEM approach for different number of elements per ply thickness for frictionless case

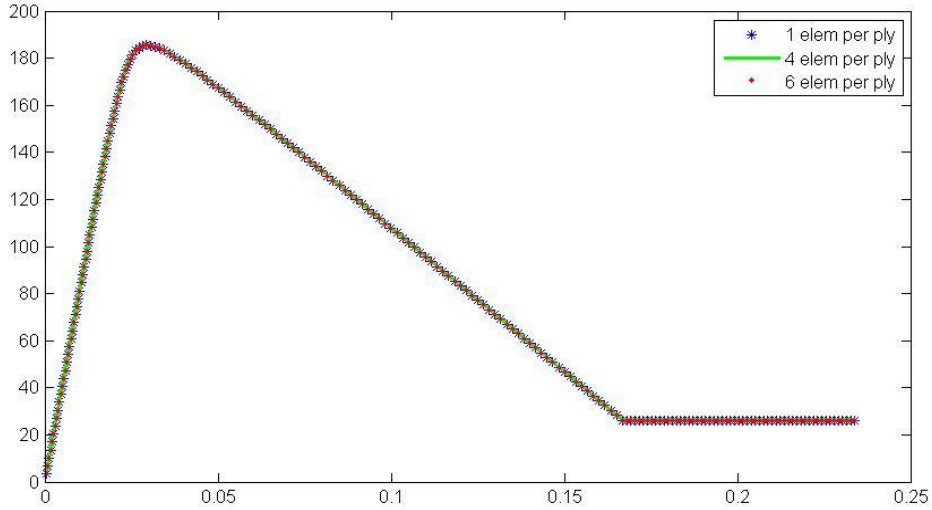

Figure 4-15: Mesh convergence for the XFEM approach for different number of elements per ply thickness for the combined damage and friction

Mesh deformations for the XFEM approach with different mesh sizes are shown in Figure 4-16. As can be seen, unlike the standard FEM, the mesh does not require to be aligned with the crack orientation. In addition, a detailed geometrical representation of the transverse deformation, forming a distinct wedge, is observed.

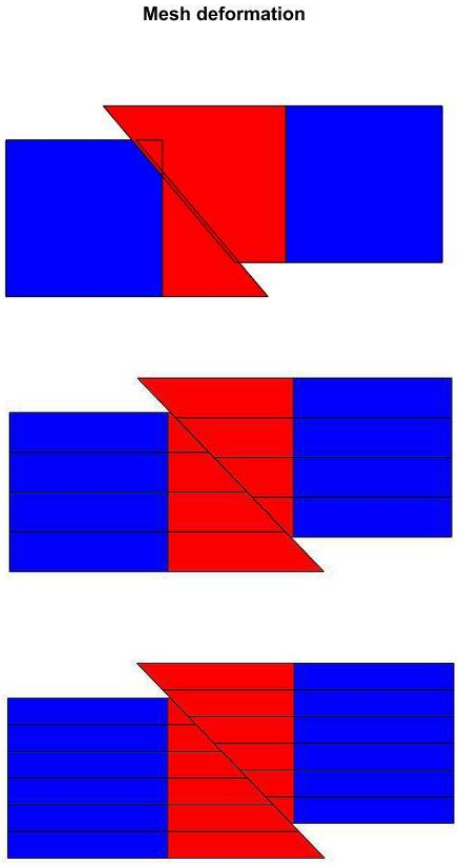

Figure 4-16: Mesh deformation for the XFEM approach for 1, 4, and 6 elements per ply thickness

5 Discussion

Choice of element types and element deletion

The comparison between different linear brick elements illustrated in Figure 4-8 indicates that the numerical prediction from cases with C3D8R and C3D8I elements are nearly indistinguishable up to the strain level of 0.06, which corresponds to the point where hourglassing causes the artificial energy over strain energy to exceed 5%. Thereafter, the results of reduced integration elements are considered not reliable and the predictions begin to deviate from each other. Fully integrated elements do not suffer from hourglassing, but with the use of more integration points, several similar or different fracture planes may be predicted in each element that could cause element locking. In addition, the deformations between C3D8R and C3D8I demonstrates no major difference, see Figure 4-9, but fully integrated elements require significantly more computational resources. For the case of C3D8R with enhanced hourglass control, the stress-strain curve shows a much stiffer response in comparison to the other cases. This indicates that the elements in the ply are more constrained; subsequently this leads to an unrealistic single ply response where the strain localization is not adequately captured, see Figure 4-9. From Figure 4-7 it is seen that using one C3D8R element through the ply thickness excluding non-linear geometry effects can predict the complete material response without hourglassing effect.

Element deletion occurs when an element is fully damaged i.e. the damage variable is equal to one. The element deletion is initiated and propagated as illustrated in Figure 4-10, where a row of elements is deleted during the same load step, which causes the total and immediate stress drop. For the peak load estimation, the simulation including element deletion provides sufficient results. However, it does not predict the remaining material response and is therefore not suitable for the case of matrix cracks in compression.

Mesh discretization and deformations of the approaches

Comparing the results shown in Figure 4-7 and Figure 4-14, it is seen that the mesh convergence is achieved with the XFEM approach, whilst the smeared crack approach does not exhibit the property of mesh objectivity. The results show that as the crack is further resolved, i.e. the number of elements through the ply thickness is increased, the peak load predictions differ and instability through oscillations increases. In general, the smeared approach is considered mesh objective, as it is mesh independent for in-plane mesh refinements as described in Section 2.3.2. However, for comparison purposes with XFEM, the mesh is refined through the ply thickness and the limits of the theory behind the smeared crack approach are evaluated. As the results show, the smeared crack approach is able to predict the material response without oscillations and issues with hourglassing when the mesh discretization is one C3D8R element per ply excluding non-linear geometry effects. On the other hand, the XFEM results for different mesh discretization are identical, which indicates the XFEM to be mesh objective, and is able to resolve the crack.

One key aspect of matrix cracks formed under transverse compression, is the forming of a wedge that can initiate and drive delamination growth. From Figure 4-16, the XFEM transverse deformation successfully generates a detailed geometrical representation of a distinct wedge. The smeared crack approach however, comparing

the deformations for different mesh discretization illustrated in Figure 4-2 and Figure 4-6, shows difficulties in capturing shearing deformations as the crack is smeared over the entire damaged elements. Yet, more elements through ply thickness does indicate that the smeared approach could geometrically represent a deformation resembling a wedge. However, increased hourglassing, and subsequently, high artificial energy makes the simulation unreliable quite soon after the peak load.

Peak load predictions and damage evolutions

The results of the frictionless cases for the XFEM and the smeared crack approach are illustrated for one element per ply in Figure 4-12. Although the damage evolutions are drastically different, both approaches exhibit near identical predictions in the bilinear material response. The differences in damage evolution can largely be attributed to the differing kinematics of the two approaches. For the smeared crack approach, the damage evolution is driven by the shearing strain along the crack surface, as stated in Equation (34), and grows more gradually due to kinematical constraints by the bulk behavior in the domain. In contrast, XFEM explicitly describes kinematics at the crack interface through a cohesive zone model, where the damage evolution is instead driven by the displacement jump in the shearing crack direction, as illustrated in Equation (48). The shearing displacement jump at the crack then causes failure and damage to localize and grow more rapidly. Both approaches ultimately succeed in predicting the same material degradation and energy dissipation regardless of the differences in the damage evolutions.

Comparing the results from the XFEM and the smeared crack approach for the cases where frictional effects are included, illustrated for one element per ply in Figure 4-13, the predicted peak load by the XFEM is approximately 20% higher than that of the smeared crack approach. However, with the increase of elements through the ply thickness, the peak load prediction of the smeared crack approach increases and is then more similar to that of the XFEM, see Figure 4-7 and Figure 4-13. Regardless, the difference in peak load predictions between the XFEM and the smeared crack approach is mainly due to the differences in damage evolutions, where XFEM exhibits an accelerated increase in damage as illustrated in Figure 4-13. Considering the fact that the frictional forces acting on a crack surface are directly proportional to the damage variable, an accelerated damage evolution exhibited by XFEM results in more frictional contributions added to the crack traction in comparison to the smeared crack approach, which ultimately raises the maximum stress level.

6 Conclusion

Modeling of matrix cracks in FRP laminates under transverse compression has been conducted by two approaches known as: the XFEM approach (a discrete crack model) and the smeared crack approach (a continuum crack model). The material model developed by Gutkin & Pinho in [7] is implemented to represent the material degradation, in which the damage development is coupled with the friction acting on the generated crack interfaces.

The pure study of the element types shows that one linear brick element (C3D8R) with reduced integration scheme, without element deletion and non-linear geometry effects, effectively predicts the material response. This significantly requires lower computational effort than fully integrated elements without experiencing element locking or hourglassing, and is therefore recommended for Abaqus/Explicit implementation of the smeared crack model in a FRP ply under pure compressive loading.

The mesh refinement study through the thickness of the ply indicates that XFEM is able to resolve the crack effectively and provides unique results regardless of mesh discretization. The XFEM approach is thus mesh objective. The smeared crack approach successfully predicts the material response with one element per ply, but shows different peak load predictions and instabilities as the crack is further resolved through mesh refinement. However, considering the fact that the investigation of failures in composite plies is normally conducted on the meso-scale, i.e. ply thickness scale, both approaches with a mesh including only one element per ply are able to produce adequate results.

The results of the frictionless cases comparison when the mesh discretization is one element through the ply thickness indicate that while the damage evolution is significantly different in the XFEM and the smeared crack approach due to differing kinematics, they both predict a near identical material linear stiffness softening and energy dissipation during the damage process effectively.

For the case where damage is combined with the frictional effects, the XFEM approach predicts the peak load approximately 20% higher than the smeared crack approach with the mesh consisting of one C3D8R element per ply. The difference is a result from the XFEM having an accelerated damage evolution, which is then directly proportional to the predicted frictional contribution. Consequently, a higher frictional contribution is added to the crack traction upon damage initiation in the XFEM approach which leads to the higher maximum stress level in the material.

The deformations of the both approaches indicate that the smeared crack approach requires more elements through the ply thickness to represent a geometry resembling a wedge. The XFEM approach however, successfully predicts the geometrical representation of matrix cracks formed under transverse compression that results in a distinct wedge, regardless of mesh discretization, which is of interest for further studies on FRP laminate failures concerning delamination, crack propagation and crack migration.

7 Future works

Explicit modeling of cracks in the XFEM approach facilitates further investigation on failures in composite laminates. To examine any benefits of a more detailed description of ply cracks, the prediction capabilities of the smeared crack and the XFEM approaches should be further evaluated. For this purpose, several possible comparisons could prove to be of interest:

Assess the predictions from both methods involving the mechanics of delamination in a composite laminate. The smeared crack approach, being a continuum material model, shows difficulties in capturing the geometrical wedge effect in matrix cracks which is of interest when considering delamination crack initiation. However, by utilizing the explicit crack description of XFEM, this interaction can be more properly captured where XFEM is proven to properly produce a detailed geometrical representation of the wedge. The development of additional cohesive zone models between plies to account for inter-laminar effects between the wedge and adjacent plies, and can prove to be valuable when predicting crack propagation, crack migration and progressive failure in composite laminates, as the better kinematics offered by XFEM should provide a better representation of the processes.

To further relate the study to continued research within applications such as crash, the modeling work done needs to be extended by including non-linear geometrical effects with large strains and rotations.

The extended finite element method is constructed and implemented in a 2D model through MATLAB. It would be of further interest to extrapolate and apply the method in 3D, as well as to evaluate additional failure mode predictions in comparison to the smeared crack approach, in order to increase the robustness of the model and the applicability of the method.

8 References

[1] P. Mallick, Fiber-reinforced composites, materials, manufacturing, and design, CRC Press, 2007.

[2] W. V. P. Joris Degrieck, "Fatigue damage modeling of fiber-reinforced composite materials: Review," *American society of mechanical engineers,* vol. 54, pp. 279-300, 2001.

[3] D. R. G. B. G. M. A. Scattina, "Investigation of creep phenomenon on composite material for bolt," *Composite structures,* vol. 134, pp. 378-383, 2015.

[4] S. Mohammadi, XFEM fracture analysis of composites, Wiley, 2012.

[5] F. v. d. M. L. S. W. Steenstra, "An efficient approach to the modeling of compressive transverse cracking in composite laminates," *Composite structures,* vol. 128, pp. 115-121, 2015.

[6] M. Jirasek, Modeling of localized inelastic deformation, Prague: Czech Technical University, 2010.

[7] S. P. R. Gutkin, "Combining damage and friction to model compressive damage growth in fibre-reinforced composites," *Journal of composite materials,* vol. 49, pp. 2483-2495, 2015.

[8] J. A. H. Ireneusz Lapczyk, "Progressive damage modeling in fiber-reinforced materials," *Composites,* vol. 38, pp. 2333-2341, 2007.

[9] S. P. R. Gutkin, "Practical application of failure models to predict the response of composite structures," in *18th International Conference on composite materials,* London.

[10] M. Uustalu, "Crush simulation of carbon/epoxy NCF composites - Development of a validation test for material models," Swerea SICOMP, Möndal, 2015.

[11] L. B. K. C. B.D. Agarwal, Analysis and performance of fiber composites, New Jersy: Wiley, 2006.

[12] R. I. Borja, "A finite element model for strain localization analysis of strongly discontinuous felds based on standard Galerkin approximation," *Computer methods in applied mechanics and engineering,* vol. 190, pp. 1529-1549, 1999.

[13] Z. P. Bazant, "Crack band theory for fracture of concrete," *Materials and structures,* vol. 16, pp. 155-177, 1983.

[14] T. B. T.P. Fries, The extended/ generalized finite element method: An overview of the method and its applications, 2009, pp. 253-304.

[15] M. B. T.P Fries, "Crack propagation with the XFEM and hybrid explicit-implicit crack description," 2011.

[16] J. Chessa, H. Wang and T. Belytschko, "On the construction of blending elements for local partition," *INTERNATIONAL JOURNAL FOR NUMERICAL METHODS IN ENGINEERING,* no. 57, pp. 1015-1038, 2003.

[17] R. Gracie, H. Wang and T. Belytschko, "Blending in the extended finite element method by discontinuous," *INTERNATIONAL JOURNAL FOR NUMERICAL METHODS IN ENGINEERING,* no. 74, pp. 1645-1669, 2007.

[18] S. Fernández-Méndez and A. Huerta, "Imposing essential boundary conditions," *Comput. Methods Appl. Mech. Engrg,* no. 193, pp. 1257-1275, 2004.

[19] G. Zi and T. Belytschko, "New crack-tip elements for XFEM and applications," *INTERNATIONAL JOURNAL FOR NUMERICAL METHODS IN ENGINEERING,* no. 57, pp. 2221-2240, 2003.

[20] T.-P. Fries and A. Zilian, "The Extended Finite Element Method (XFEM)," 2009.

[21] J. Tarancón, A. Vercher, E. Giner and F. Fuenmayor, "Enhanced blending elements for XFEM applied to linear elastic," *INTERNATIONAL JOURNAL FOR NUMERICAL METHODS IN ENGINEERING,* no. 77, pp. 126-148, 2008.

[22] K. Shibanuma and T. Utunomiya, "Reformulation ofXFEMbasedonPUFEMforsolvingproblemcaused," *Finite ElementsinAnalysisandDesign,* no. 45, pp. 806-816, 2009.

[23] H. Waisman and T. Belytschko, "Parametric enrichment adaptivity by the extended finite," *International Journal for Numerical Methods in Engineering,* no. 73, pp. 1671-1692, 2008.

[24] K. Park and G. H. Paulino, "Cohesive Zone Models: A Critical Review of Traction-Separation Relationships Across Fracture Surfaces," *Applied Mechanics Reviews,* no. 64, 2011.

[25] Y. Wang and H. Waisman, "Progressive delamination analysis of composite materials unsing XFEM and a discrete damage zone model," *Compute Mech,* no. 55, pp. 1-26, 2015.

[26] H. Espinosa, S. Dwivedi and H.-C. Lu, "Modeling impact induced delamination of woven fiber reinforced composites with contact/cohesive laws," *Commput. Methods Appl. Mech. Engrg. ,* no. 183, pp. 259-290, 2000.

[27] A. Giulio, "On the influence of the shape of the interface law on the applicatoin of cohesive-zone models," *Composites Science and Technology,* no. 66, pp. 723-730, 2006.

[28] M. Elices, G. Guinea, J. Gómez and Planas.J, "The cohesive zone model: advantages, limitations and challenges," *Engineering Fracture Mechanics,* no. 69, pp. 137-163, 2002.

[29] Dassault-Systemes, "Abaqus 6.14 Online Documentation," 23 April 2014. [Online]. Available: http://abaqus.me.chalmers.se/texis/search/?query=artificial+energy+limit&submit.x=0&submit.y=0&group=bk&CDB=v6.14.

[30] J. R. A. N. M. A. R. de Borst, "Discrete vs smeared crack models for concrete fracture," *International journal for numerical and analytical methods in geomechanics,* pp. 583-607, 2004.

[31] L. L. P. R. S.T. Pinho, "Physically-based failure models and criteria for laminated fibre reinfoced composites with emphasis on fibre kinking part I development," Imperial college London, London.

[32] H. S. A. Puck, "Failure analysis of FRP laminates by means of physically based phenomenological models," *Composites science and technology,* vol. 62, pp. 1633-1662, 2002.

[33] H. S. A. Puck, "Failure analysis of FRP laminates by means of physically based phenomenological models," *Composites science and technology,* vol. 58, pp. 1045-1067, 1998.